NASA CONTRACTOR
REPORT

NASA CR-2

2. u/u

CONSOLIDATION OF FATIGUE AND
FATIGUE-CRACK-PROPAGATION DATA
FOR DESIGN USE, FINAL REPORT

Richard C. Rice, Kent B. Davies,
Carl E. Jaske, and Charles E. Feddersen

Prepared by
BATTELLE COLUMBUS LABORATORIES
Columbus, Ohio 43201
for Langley Research Center

NATIONAL AERONAUTICS AND SPACE ADMINISTRATION • WASHINGTON, D. C. • OCTOBER 1975

5.

1. Report No. NASA CR-2586	2. Government Accession No.	3. Recipient's Catalog No.
4. Title and Subtitle Consolidation of Fatigue and Fatigue-Crack-Propagation Data for Design Use		5. Report Date October 1975
		6. Performing Organization Code
7. Author(s) Richard C. Rice, Kent B. Davies, Carl E. Jaske, and Charles E. Feddersen		8. Performing Organization Report No.
		10. Work Unit No.
9. Performing Organization Name and Address Battelle Memorial Institute Columbus Laboratories 505 King Avenue Columbus, OH 43201		11. Contract or Grant No. NAS1-13358
12. Sponsoring Agency Name and Address National Aeronautics and Space Administration		13. Type of Report and Period Covered Contractor Report
		14. Sponsoring Agency Code

15. Supplementary Notes

Final report.

16. Abstract

Analytical methods have been developed for consolidation of fatigue and fatigue-crack-propagation data for use in design of metallic aerospace structural components. To evaluate these methods, a comprehensive file of data on 2024 and 7075 aluminums, Ti-6Al-4V alloy, and 300M steel was established by obtaining information from both published literature and reports furnished by aerospace companies. Analyses were restricted to information obtained from constant-amplitude load or strain cycling of specimens in air at room temperature.

Both fatigue and fatigue-crack-propagation data were analyzed on a statistical basis using a least-squares regression approach. For fatigue, an equivalent strain parameter was used to account for mean stress or stress ratio effects and was treated as the independent variable; cyclic fatigue life was considered to be the dependent variable. An effective stress-intensity factor was used to account for the effect of load ratio on fatigue-crack-propagation and was treated as the independent variable. In this latter case, crack-growth rate was considered to be the dependent variable. A two-term power function was used to relate equivalent strain to fatigue life, and an arc-hyperbolic-tangent function was used to relate effective stress intensity to crack-growth rate.

17. Key Words (Suggested by Author(s))		18. Distribution Statement	
Fatigue life Fatigue-crack-propagation rate Constant amplitude loading Data consolidation Regression analyses 2024 aluminum	7075 aluminum Ti-6Al-4V titanium 300M steel	Unclassified – Unlimited Subject Category 39 Structural Mechanics	
19. Security Classif. (of this report) Unclassified	20. Security Classif. (of this page) Unclassified	21. No. of Pages 75	22. Price* $4.25

CONTENTS

ILLUSTRATIONS

TABLES

CONSOLIDATION OF FATIGUE AND FATIGUE-CRACK-

PROPAGATION DATA FOR DESIGN USE

By Richard C. Rice, Kent B. Davies,
Carl E. Jaske, and Charles E. Feddersen
Battelle's Columbus Laboratories

SUMMARY

Analytical methods have been developed for consolidation of fatigue and fatigue-crack-propagation data for use in design of metallic aerospace structural components. To evaluate these methods, a comprehensive file of data on 2024 and 7075 aluminums, Ti-6Al-4V alloy, and 300M steel was established by obtaining information from both published literature and reports furnished by aerospace companies. Analyses were restricted to information obtained from constant-amplitude load or strain cycling of specimens in air at room temperature.

Both fatigue and fatigue-crack-propagation data were analyzed on a statistical basis using a least-squares regression approach. For fatigue, an equivalent strain parameter was used to account for mean stress or stress ratio effects and was treated as the independent variable; cyclic fatigue life was considered to be the dependent variable. An effective stress-intensity factor was used to account for the effect of load ratio on fatigue-crack propagation and was treated as the independent variable. In this latter case, crack-growth rate was considered to be the dependent variable. A two-term power function was used to relate equivalent strain to fatigue life, and an arc-hyperbolic-tangent function was used to relate effective stress intensity to crack-growth rate.

Smooth-specimen and notched-specimen fatigue data were treated separately. Data for various types of notches and theoretical stress-concentration factors were consolidated by using a local stress-strain approach. Both cyclic and monotonic stress-strain curves were employed in calculating the local stress-strain response from nominal loading information. Fatigue-crack-propagation data from various types of specimens were treated by using stress-intensity factors with appropriate geometric scaling functions.

INTRODUCTION

Fatigue has long been an important consideration in the design of air-
craft structures and recent experience with modern aerospace structures has
emphasized the importance of considering both fatigue and fatigue-crack propa-
gation in the design and service performance of aircraft. For conventional
static properties of metallic materials, data are consolidated and presented
in the form of statistically based design allowable information in documents
such as MIL-HDBK-5B (ref. 1). For fatigue and fatigue-crack propagation, how-
ever, such consolidated presentations of data and design allowable information
are usually not available and the data are presented in terms of typical or
average values.

Part of the problem for fatigue and fatigue-crack propagation is that
these behaviors are influenced by a wide range of parameters that include cy-
clic stress, mean stress, cyclic frequency, temperature, environment, product
form and orientation with respect to loading, structural geometry (size,
shape, and notch configuration), metallurgical and surface effects associated
with heat treatment, microstructure, and machining practices. Most aerospace
companies tend to generate data for a limited number of these many variables
to fulfill specific local design needs. Much of this information is retained
within each company, and that which becomes available in open literature is
often digested in accordance with particular theoretical considerations and
analytical procedures endemic to a given organization. Since these considera-
tions and procedures vary among companies, it is difficult to effect a system-
atic consolidation of such data. Assessment of fatigue and fatigue-crack-
propagation data is further complicated by the fact that there have been no
standard methods for these types of testing. Recommended standard procedures
for high-cycle fatigue testing under nominally elastic cyclic loading have
just recently been published (ref. 2). Similar recommended standard proce-
dures are still being developed for low-cycle fatigue testing where conditions
of cyclic inelastic deformation are present and for fatigue-crack-propagation
testing.

In this study, work was directed toward systematizing and consolidating
available fatigue and fatigue-crack-propagation information on 2024 and 7075

aluminum alloys, Ti-6Al-4V alloy, and 300M steel. Fracture information on these same alloys and on D6AC steel were tabulated and graphically summarized as described in detail in reference 3, but were omitted from the present effort. It was considered imperative that the analytical procedures be compatible with statistical methods of data presentation. Similar approaches were used for both fatigue and fatigue-crack propagation, as illustrated in figure 1. The logarithm of fatigue life was the dependent variable in both cases. An equivalent strain parameter similar to that suggested by Walker (ref. 4) and Smith, et al (ref. 5) was used to account for stress ratio effects and was treated as an independent variable in the fatigue analysis. A similar effective stress-intensity factor (ref. 4) was used to account for stress ratio effects and was treated as the independent variable in the fatigue-crack-propagation analysis.

Fatigue-crack propagation is more complicated than fatigue because different life curves (fig. 1) are obtained for each different state of initial damage. Thus, fatigue-crack-propagation results are usually presented in terms of crack-growth rate as shown schematically in figure 2. The layering of rate data as a function of stress ratio can be accounted for using the effective stress-intensity concept mentioned above.

The main body of this report is divided into three sections. Handling of the data is briefly discussed in the first section. A very detailed description of the data handling system is contained in reference 3. Analyses of fatigue and fatigue-crack-propagation behavior are covered in the other two sections. Analytical details and results for each type of behavior are discussed separately in its respective section.

SYMBOLS

A   constant used to define weighting function for fatigue data

a   half-crack length for center-cracked specimen, m (in.)

$d(2a)/dN$ fatigue-crack-growth rate, m/cycle (in./cycle)

B_0, B_1, B_2 regression coefficients

b   fatigue strength exponent
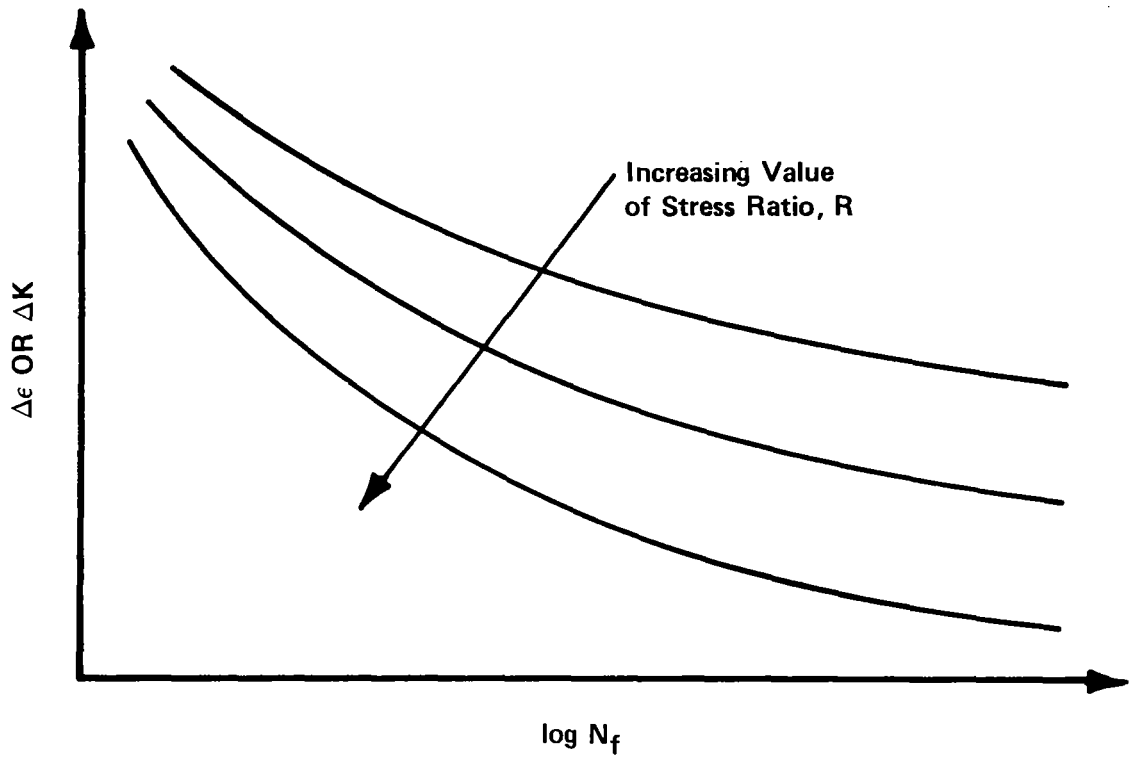
FATIGUE ANALYSIS, ϵ_{eq}

$\log N_f = f [\Delta\epsilon, R]$

or specifically,

$\log N_f = f [\Delta\epsilon^m (\sigma_{max}/E)^{1-m}]$

FATIGUE CRACK
PROPAGATION ANALYSIS, K_{eff}

$\log N_f = f [\Delta K, R]$

or specifically,

$\log N_f = f [\Delta K^m K_{max}^{1-m}]$

m may be treated as a material parameter

Figure 1. — Similarity between fatigue and fatigue-
crack-propagation analyses.
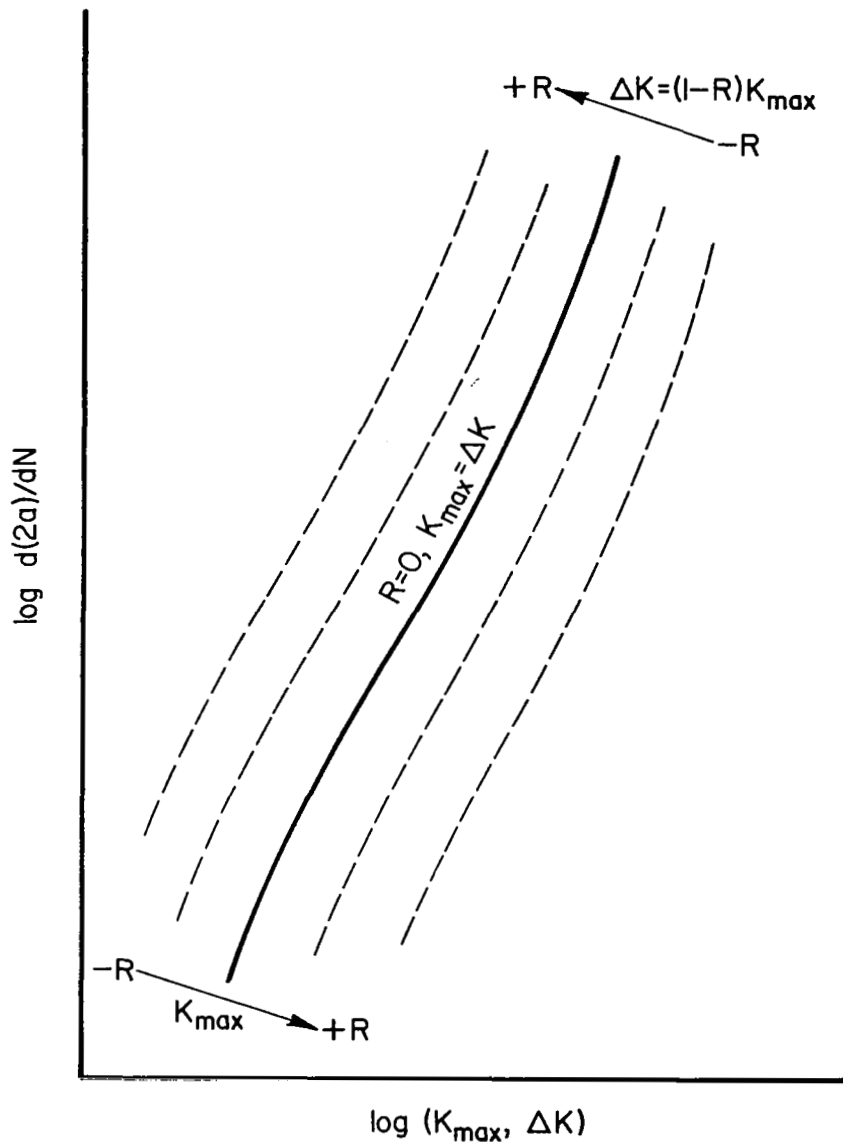
Figure 2. — Schematic illustration of layering in fatigue-crack-propagation rate data for a center-cracked specimen.

C_1, C_2	regression coefficient in arc-hyperbolic-tangent relation
c	fatigue ductility exponent
E	elastic modulus, MN/m^2 (ksi)
e_a	nominal strain amplitude
e_{max}	maximum nominal strain
$f(\ )$	function notation
$f_c(\ )$	cyclic stress-strain behavior function
$f_m(\ )$	monotonic stress-strain behavior function
i	subscript, index notation for ith value
K	stress-intensity factor, $MN/m^{3/2}$ (ksi $\sqrt{in.}$)
ΔK	stress-intensity-factor range, $MN/^{3/2}$ (ksi $\sqrt{in.}$)
K'	cyclic strength coefficient, MN/m^2 (ksi)
K_c	critical fracture toughness, $MN/m^{3/2}$ (ksi $\sqrt{in.}$)
K_{eff}	effective stress-intensity factor, $MN/m^{3/2}$ (ksi $\sqrt{in.}$)
K_f	fatigue strength reduction factor
K_{max}	maximum stress-intensity factor, MN/m^2 (ksi $\sqrt{in.}$)
K_0	threshold stress-intensity factor, MN/m^2 (ksi $\sqrt{in.}$)
K_t	theoretical stress concentration factor
K_ϵ	strain concentration factor
K_1, K_2	strength coefficients, MN/m^2 (ksi)
k	Stulen-type equivalent strain coefficient

6

$k_{u,\nu}$ one-sided tolerance limit factor for a normally distributed variable with n - 2 degrees of freedom at level u and the desired confidence ν

m   equivalent strain and equivalent stress-intensity exponent

m_1, m_2 exponents in optimized fatigue-life expression

N   number of cycles

N_f number of cycles to failure

$N_{f_{90}}$, $N_{f_{99}}$ 90 and 99 percent survival estimates of fatigue life

n   sample population

n' cyclic strain hardening exponent

n_1, n_2 strain hardening exponents

R   stress ratio

R^2 correlation coefficient squared

r   notch root radius, mm (in.)

S   nominal stress, MN/m^2 (ksi)

S_a nominal stress amplitude, MN/m^2 (ksi)

S_m mean nominal stress, MN/m^2 (ksi)

S_{max} maximum nominal stress, MN/m^2 (ksi)

s_y sample standard deviation of Y

$s_{y \cdot x}$ standard error of estimate

U( )   stress ratio function

u	desired tolerance level — indicates the percentage of occurrences (or nonoccurrences) which are expected ν percent of the time
V	variance
V_o	variance of a fatigue data sample for $N_f < 10^5$
W	panel width, mm (in.)
$W(\log N_f)$	weighting function applied to fatigue data
X	independent variable in regression equation
Y	dependent variable in regression equation
$\overline{Y}$	mean value of Y
α	mean stress exponent
$\Delta\epsilon$	local strain range
ϵ_a	local strain amplitude
$\epsilon_a(1)$, $\epsilon_a(2)$	specific values of ϵ_a used to define stress-strain curve
ϵ_f'	fatigue ductility coefficient
ϵ_{eq}	equivalent strain
ϵ_{max}	maximum local strain
$\Delta\epsilon_p$	local plastic strain range
ν	desired confidence level in determination of tolerance limits, a 95 percent level is commonly used
ρ	notch analysis material constant, mm (in.)
$\Delta\sigma$	local stress range

σ_a local stress amplitude

$\sigma_a(1)$, $\sigma_a(2)$ specific values of σ_a defining stress-strain curve, MN/m^2 (ksi)

σ_f' fatigue strength coefficient, MN/m^2 (ksi)

σ'_{max} initial local maximum stress in a notched specimen, MN/m^2 (ksi)

σ_m mean local stress, MN/m^2 (ksi)

σ_{max} maximum local stress, MN/m^2 (ksi)

DATA HANDLING

To implement the evaluation of existing fatigue and fatigue-crack-propagation data, an extensive survey was made of the literature and of aerospace companies that might have unpublished internal reports. A computerized system was developed to compile and store data obtained from this survey. A more detailed discussion of the data handling efforts was included in reference 3.

Acquisition

In this program, fatigue data from uncracked smooth or notched specimens were treated separately from fatigue-crack-propagation data from precracked specimens. Reaching total fracture under cyclic loading involves both fatigue-crack initiation and propagation. As shown in figure 3, crack-initiation life can vary considerably, depending upon the definition of a crack. The wide range of sizes, 2.54×10^{-4} mm to 2.54 mm (10^{-5} to 10^{-1} inch), considered to be cracks by various investigators causes an ill-defined area of overlap between initiation and propagation. In most fatigue tests of small specimens of virgin material, the initiation phase is generally considered to be a more significant portion of cyclic life than the propagation phase. Thus, it was assumed that the total number of cycles to failure normally reported in fatigue tests of simple specimens was a reasonable approximation of the number of cycles required to initiate an engineering size flaw. Fatigue-crack-propagation
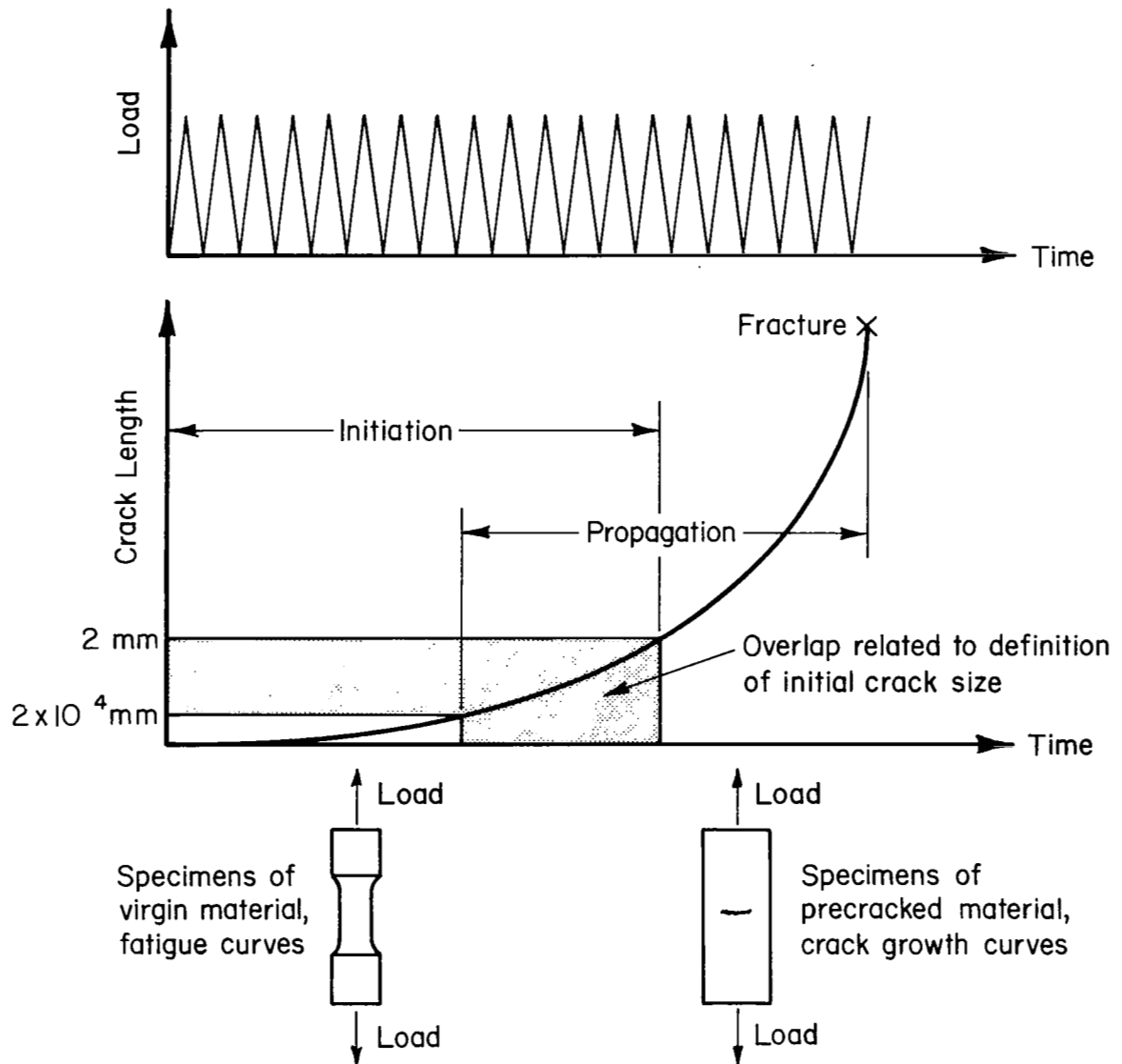
Figure 3. — Effect of definition of crack initiation on relation between fatigue-crack initiation and fatigue-crack propagation.

information was obtained from studies where cyclic crack growth was measured using a precracked sample. To give an appreciation for extent of this data acquisition task, the amount of data analyzed in this program is summarized in table 1.

TABLE 1. — SUMMARY OF AMOUNT OF DATA THAT WERE ANALYZED

Material	Number of data points	
	Fatigue	Fatigue-Crack Propagation
2024 aluminum	1181	3407
7075 aluminum	1897	1828
300M steel	507	513
Ti-6Al-4V	1145	782
Overall total	4730	6530

Information was taken both from the open literature and from company reports. Applicable reports were obtained from the technical files of the Metals and Ceramics Information Center (MCIC). Throughout the program, new reports, acquired by MCIC, were screened and added to the data base when applicable. In order to obtain as much recent information as possible, literature searches were obtained from the National Aeronautics and Space Administration and the Defense Documentation Center. In addition, pertinent reports obtained through the MIL-HDBK-5 (ref. 1) program were used.

Internal reports from aerospace companies and unpublished data were obtained from various laboratories that conduct fatigue and fatigue-crack-propagation research. A letter was prepared and sent out to members of the American Society for Testing and Materials (ASTM) Committee E09 on Fatigue. A similar letter was also sent to members of the ASTM Committee E24 on Fracture Testing of Metals and to members of the MIL-HDBK-5 (ref. 1) Coordination Group. The type of information that was requested in these letters is summarized in the following two sections.

Fatigue information. — For the alloys of interest (2024 and 7075 aluminum, Ti-6Al-4V, and 300M steel), fatigue life data were collected from constant

amplitude axial-load tests of simple specimens that reflect basic material behavior. This requirement excluded joints or components but included both notched and unnotched data, where notch configuration and severity were variables. Data for cyclic lives ranging from $>10^2$ to $<10^7$ cycles, strain- and load-controlled test data, and variable stress ratio (or mean stress) data were of interest.

Basic test data were obtained; i.e., tables of stress or strain versus lifetime. For tests involving cyclic plasticity, cyclic stress-strain information in the form of stress and strain as a function of loading history were requested. The cyclic stress-strain information which was obtained is included in Appendix A.

Fatigue-crack-propagation information. — Fatigue-crack-propagation data were collected for center-cracked panels (in a variety of widths), part-through-cracked or surface-flawed specimens, compact-tension specimens, and double-cantilever-beam specimens. Basic test data again were desired; i.e., tabular displays of crack size versus cycles. Delineation of the stress cycle employed for each test, as well as test frequency, was necessary. In some cases, multiple tests were conducted on a single specimen such that propagation occurred on successive crack-growth segments under different cyclic-stress conditions. Each of these conditions was considered as a single test in the analysis.

Recording and Storage

Information used in this program was stored in a format suitable for computerized analysis. Detailed data were recorded on punched cards as described in reference 3. A computer program was written to store these data on magnetic tape. The storage program writes the data in card image format on seven-track magnetic tape at a density of 800 bits per inch. The tape was organized as a number of data files which divided the data with respect to type of material and type of data. Table 2 presents the data files and respective file number for retrieval purposes. Specific data could be accessed by utilizing a tape-handling control statement to skip to the referenced file number. A duplicate data listing was written on the tape as a back-up source of data. The use of magnetic tape provided a compact source of fatigue and fatigue-crack-propagation data.

12

TABLE 2. — ORGANIZATION OF DATA TAPE

File No.	Material	Product Form	Specimen Type[a]	File No.	Material	Product Form	Specimen Type[a]
Fatigue-Crack-Propagation Data				Fatigue Data (Continued)			
1	7075-T7351	Sheet	CC	27	2024-T4	Extrusion	S
2	7075-T6	Sheet, Clad	CC	28	2024-T4	Extrusion	CR
3	7075-T6	Sheet	CC	29	2024-T351	Plate	EN
4	2024-T3	Sheet, Clad	CC	30	300M	Billet	S
5	2024-T3	Sheet	CC	31	300M	Billet	CR
6	300M	Plate	CC	32	300M	Forging	S
7	Ti-6Al-4V	Sheet	CC	33	300M	Forging	CR
8	Ti-6Al-4V	Forging, STA	CT	34	Ti-6Al-4V	Sheet, Annealed	S
9	Ti-6Al-4V	Forging, STA + Annealed	CT	35	Ti-6Al-4V	Sheet, Annealed	EN
Fatigue Data				36	Ti-6Al-4V	Sheet, STA	S
				37	Ti-6Al-4V	Sheet, STA	CN
10	7075-T6	Sheet	S	38	Ti-6Al-4V	Sheet, STOA	S
11	7075-T6	Sheet	EN	39	Ti-6Al-4V	Sheet, STOA	EN
12	7075-T6	Sheet	CN	40	Ti-6Al-4V	Plate, STA	S
13	7075-T6	Sheet	FN	41	Ti-6Al-4V	Plate, STA	EN
14	7075-T6	Sheet, Clad	S	42	Ti-6Al-4V	Forging, Annealed	S
15	7075-T6	Extrusion	S	43	Ti-6Al-4V	Forging, Annealed	CR
16	7075-T6	Bar and Rod	S	44	Ti-6Al-4V	Forging, STA	S
17	7075-T6	Bar	CR	45	Ti-6Al-4V	Casting, Annealed	S
18	7075-T651	Bar	CR	46	Ti-6Al-4V	Casting, Annealed	EN
19	7075-T651	Bar	EN	47	Ti-6Al-4V	Casting, Annealed	CR
20	2024-T3	Sheet	S	48	Ti-6Al-4V	Casting, STA	S
21	2024-T3	Sheet	EN	49	Ti-6Al-4V	Casting, STA	CR
22	2024-T3	Sheet	CN	50	Ti-6Al-4V	Extrusion, Annealed	S
23	2024-T3	Sheet	FN	51	Ti-6Al-4V	Extrusion, Annealed	CN
24	2024-T3	Sheet, Clad	S	52	Ti-6Al-4V	Extrusion, Annealed	CR
25	2024-T4	Bar and Rod	S	53	Ti-6Al-4V	Bar, Annealed	S
26	2024-T4	Bar	CR	54	Ti-6Al-4V	Bar, Annealed	CR

[a]Specimen type abbreviations are as follows: CC = center-crack specimen; CT = compact-tension specimen; S = smooth specimen; EN = edge-notched specimen; CN = center-notched specimen; FN = fillet-notched specimen; and CR = circumferentially notched specimen.

FATIGUE ANALYSIS

Designers of aircraft structural components usually base their fatigue analysis on data from stress versus number of cycles to failure (S-N curves). Data for these S-N curves are obtained from constant-amplitude fatigue tests of simple notched and unnotched specimens. The stress value in the S-N curve is usually either S_{max} or S_a and the S-N relationship is defined for a constant value of mean stress or stress ratio. To obtain estimates of fatigue life for other values of mean stress, interpolations between existing data must be made. Average curves are often used to construct modified Goodman diagrams to aid in making these interpolations. Sets of S-N curves are normally required for both smooth specimens and for notched specimens with different notch severities.

Determination of a meaningful set of average S-N curves for a material may require 100 or more specimens. If a statistically based S-N curve is required for each condition, this number could easily increase to 500 or more. Such large amounts of data are not usually available, even for the more commonly used, well-characterized materials.

The number of specimens required to fully characterize a material's fatigue resistance would be reduced considerably, however, if data from different S-N curves could be combined to form a single curve. In many cases, such a consolidation would yield data samples large enough for statistically based life estimates.

The following subsections describe an analytical procedure for combining fatigue data generated over a range of mean stresses and/or notch concentrations. The consolidation of data generated at different mean stresses (or stress ratios) is considered first. Three equivalent strain formulations are noted and the method which provides best overall mean stress consolidations is described in detail. The consolidation of notched data is described in the next subsection and a method for estimating stable local alternating strains and maximum stress levels is reviewed. The consolidated data are analytically described in the third subsection in which statistical variations in the data are bounded by tolerance limits. The final two subsections describe the overall results and an example problem which illustrates usage of the developed fatigue analysis procedure.

14

Consolidation of Fatigue Data Generated
at Various Mean Stress Levels

It has been found that fatigue life data generated at various mean stresses can be consolidated through the use of an equivalent strain (or equivalent stress) parameter. Equivalent strain is defined by an equation relating two terms that uniquely define constant-amplitude loading conditions. One term represents the cyclic strain amplitude in terms of either $\Delta\epsilon$ or ϵ_a, while the other term defines the mean stress either directly as σ_m or indirectly as σ_{max}. In the general sense, equivalent strain has application in both notched and unnotched fatigue situations. For unnotched specimens, equivalent strain is based on nominal values of stress and strain; for notched specimens, equivalent strain values are dependent on estimates of stable local stress and strain.

Three equivalent strain parameters were reviewed in this analysis. The first was based upon a Stulen-type of formulation as reported by Jaske, et al (ref. 3) and was expressed as follows:

$$\epsilon_{eq} = \epsilon_a + k\sigma_m/E \tag{1}$$

The second was proposed by Topper and Sandor (ref. 6) and was represented by the following relationship:

$$\epsilon_{eq} = \epsilon_a + \sigma_m{}^\alpha/E \tag{2}$$

The third formulation was based on a parameter suggested by Walker (ref. 4) and was expressed in the following manner:

$$\epsilon_{eq} = (2\epsilon_a)^m (\sigma_{max}/E)^{1-m} \tag{3}$$

Initial investigations on collections of unnotched fatigue data showed that all three equivalent strain formulations provided good mean stress data consolidations, but further detailed analyses (ref. 3) revealed that equation (3) was as good or better than the other two for all cases examined.

Calculation of an equivalent strain using equation (3) required the specification of σ_{max} and ϵ_a for each specimen and a value for the material parameter, m. The majority of unnotched fatigue data available for analysis were generated under load control conditions, where values of σ_{max} were always known, but values of ϵ_a were not known for those tests involving cyclic plasticity. In these cases, the cyclically stable stress-strain curve was used to

15

estimate values of ϵ_a from known values of σ_a. This approach was reasonable for the type of materials and for the relatively small values of plastic strain amplitude encountered in the present study.

For all the materials considered in this study, it was found that the cyclic stress-strain curve could be well approximated as follows:

$$\sigma_a = E\epsilon_a, \ 0 < \epsilon_a \leq \epsilon_a(1)$$

$$\sigma_a = K_1 \epsilon_a^{n_1}, \ \epsilon_a(1) < \epsilon_a \leq \epsilon_a(2) \tag{4}$$

$$\sigma_a = K_2 \epsilon_a^{n_2}, \ \epsilon_a(2) < \epsilon_a$$

Values of the equation constants for the investigated materials are listed in table 3. Four different sets of constants are defined for Ti-6Al-4V because cyclic stress-strain properties were found to vary substantially with processing variations. When the titanium data were analyzed, the set of cyclic and monotonic values that appeared to represent most reasonably the cyclic and monotonic stress-strain response of a particular material condition were used. The data upon which these values were based are reported in references 7 through 10. An alternate and acceptable approach would have been to represent the cyclic stress-strain curve by a power function relating stress amplitude to plastic strain amplitude. In essence, any relation that adequately models the cyclic stress-strain response could be used in place of equation (4).

The value of m in equation (3) was determined for each material through a least-squares regression analysis in which a third-order polynomial in ϵ_{eq} was fit to the life data. The m value which provided the maximum consolidation of data (i.e., the minimum standard deviation) was considered optimum. Details of the statistical analysis are described in Appendix B.

A comparison of results for the investigated materials revealed that a value of m = 0.40 was nearly optimum for all materials. Specification of m at this value caused almost no increase in standard deviation for the aluminum data samples and no more than a 1-percent increase for most of the steel and titanium data collections. On this basis, an m value of 0.40 was used in all final analyses.

TABLE 3. — CONSTANTS USED TO DEFINE CYCLIC STRESS-STRAIN CURVES

Material	E, MN/m² (ksi)	K_1, MN/m² (ksi)	K_2, MN/m² (ksi)	$\sigma_a(1)$, MN/m² (ksi)	$\sigma_a(2)$, MN/m² (ksi)	$\epsilon_a(1)$	$\epsilon_a(2)$	n_1	n_2
2024-T4 Bar[a]	70 300 (10 200)	1165 (169)	676 (98)	414 (60)	572 (83)	0.0059	0.0275	0.200	0.048
2024-T3 Sheet[b]	73 100 (10 600)	5135 (745)	917 (133)	358 (52)	435 (63)	0.0049	0.0071	0.499	0.150
7075-T6 Bar[a]	71 000 (10 300)	1406 (204)	896 (130)	483 (70)	662 (96)	0.0068	0.0285	0.213	0.087
7075-T6 Sheet[b]	72 400 (10 500)	22 260 (3230)	2550 (370)	326 (47)	465 (67)	0.0045	0.0071	0.782	0.346
300M Billet[b]	199 900 (29 000)	17 370 (2520)	7240 (1050)	1140 (165)	1520 (220)	0.0057	0.0098	0.529	0.339
Ti-6Al-4V Annealed Plate[b]	110 300 (16 000)	6650 (965)	2400 (348)	618 (90)	765 (111)	0.0056	0.0098	0.458	0.240
Ti-6Al-4V Annealed Cylindrical Forging[c] (coarse microstructure)	115 100 (16 700)	8890 (1290)	2140 (310)	702 (102)	828 (120)	0.0061	0.0081	0.493	0.198
Ti-6Al-4V Annealed Hot Rolled Bar[c] (fine microstructure)	108 900 (15 800)	3915 (568)	1340 (194)	741 (107)	828 (120)	0.0068	0.0105	0.341	0.104
Ti-6Al-4V STA Bar[d]	110 300 (16 000)	7440 (1080)	1870 (272)	794 (115)	978 (142)	0.0072	0.0110	0.450	0.144

[a]Values based on data of Endo and Morrow (ref. 7) and Landgraf, et al (ref. 8).
[b]Values based on data generated by Jaske, et al (ref. 3).
[c]Values based on data of Gamble (ref. 9).
[d]Values based on data of Smith, et al (ref. 10).

Consolidation of Fatigue Data Generated at
Various Stress Concentration Levels

Consolidation of notched-specimen fatigue data was handled in a manner directly analogous to that used for the unnotched specimens, except that estimates of stable local stress and strain at the notch root were used in place of nominal values in the determination of equivalent strains. The following paragraphs outline the analytical procedure developed for the estimation of local maximum stresses and alternating strains in notched specimens subjected to constant-amplitude, nominal-stress cycling.

Smooth specimen simulations of local stress-strain behavior in notched specimens (ref. 11) have indicated that combined cyclic hardening (or softening) and cyclic stress relaxation often occur at the notch tip when nominal stresses are sufficiently large to cause localized cyclic plastic deformations. To estimate stable local values of alternating stress and strain from nominal values, it is necessary to compensate for this combined hardening and relaxation. Research (refs. 12 through 15) has shown that the effects of cyclic hardening or softening can be accounted for by using a cyclic stress-strain curve in combination with nominal alternating strain values modified by an appropriate notch-concentration factor such as K_t, K_f, or K_ϵ.

All three modifying factors were investigated in this study to determine which one gave the most reasonable indication of local strain concentration. Values of K_t were based on information obtained from charts such as those in Peterson's handbook (ref. 16), and values of K_f were computed from an empirical relation as described below. Neuber's rule (ref. 17) was used with both K_t and K_f in calculating values of K_ϵ. The degree to which notched-specimen fatigue data of various K_t's and notch types were consolidated was used as a measure of how well local strain was estimated.

After completion of the comparative analysis (ref. 3), it was concluded that K_f, when used in the form

$$\epsilon_a = K_f \, e_a \qquad\qquad (5)$$

as a simple strain multiplication factor, provided the best overall consolidations of notched data for the investigated materials. Several forms of K_f were available, but the following relation proposed by Peterson (ref. 18)

18

$$K_f = 1 + \frac{K_t - 1}{1 + \rho/r} \tag{6}$$

was chosen because it was simple and has been shown (ref. 19) to work reasonably well in comparison to other K_f formulations.

Once a value of ε_a was computed, according to equation (5), it was necessary to compute the corresponding value of σ_{max}. Potential localized cyclic hardening or softening in combination with cyclic relaxation of mean stress made it impossible to compute σ_{max} directly from nominal maximum stress values. It was found, however, that a local maximum stress could be well approximated by considering that the notch root was subject to constant-strain cycling. Thus, the local maximum stress produced by the first constant-amplitude nominal-stress cycle was definable in terms of the monotonic stress-strain curve, and subsequent changes in σ_{max} (for a constant maximum strain) were attributable to cyclic changes in local stress amplitude. This concept is illustrated in figure 4, where the monotonic and cyclic stress-strain curves for a typical cyclically hardening alloy are shown. According to the concept described, initial local stresses would follow the monotonic curve to its peak value of stress, σ'_{max}, and strain, ε_{max}. The local maximum strain ε_{max} is approximated by

$$\varepsilon_{max} = K_f e_{max} \tag{7}$$

and σ'_{max} is found from ε_{max} and the monotonic stress-strain curve. Combined cyclic hardening (in this case) and mean stress relaxation would subsequently occur because of localized cyclic inelastic strains. The magnitude of change in σ'_{max} could be approximated by the change in stress amplitude during local strain cycling. This change (indicated by A in figure 4) denotes the magnitude of shift in the local stress-strain loop from the initial condition, σ'_{max}, to the final condition, σ_{max}. It can be seen that this method predicts no change in local maximum stress from that defined by the monotonic curve, unless there is some localized cyclic plasticity. This behavior has been noted in some of the smooth specimen notch simulations mentioned earlier (ref. 11). Analytically, this approximation procedure can be expressed as follows:

$$\sigma_{max} = \sigma'_{max} + [f_c(\varepsilon_a) - f_m(\varepsilon_a)] \tag{8}$$

19
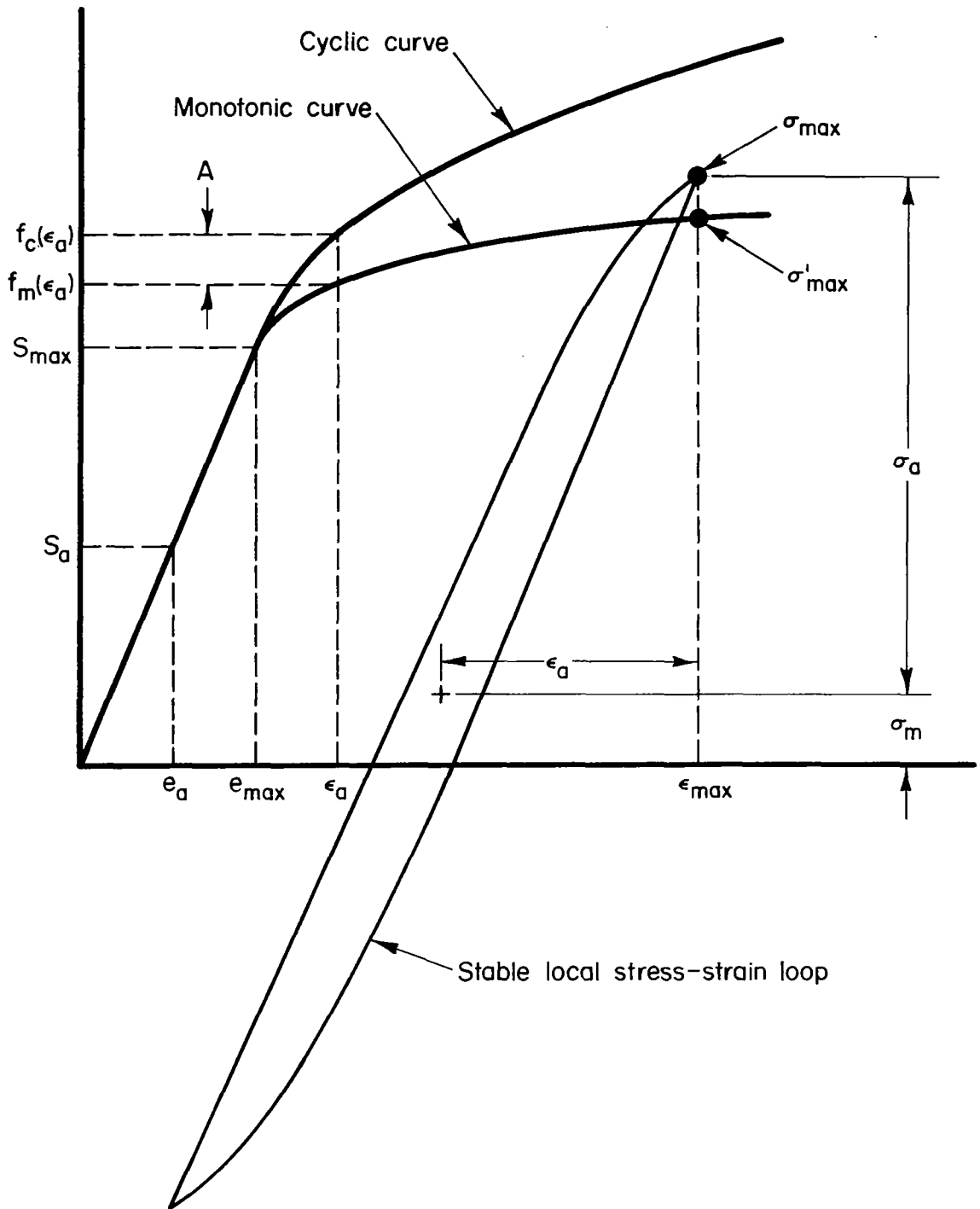
Figure 4. — Schematic illustration of an analytically approximated
stable stress-strain loop after combined cyclic
hardening and mean stress relaxation.

where f_m and f_c represent equation (4) for the monotonic and cyclic stress-strain curves, respectively. The constants used to define the monotonic curves are given in table 4. It should be noted that equation (8) is an empirical relationship that was found to work well for constant-amplitude loading where most of the cyclic life was at the stable relaxed local mean stress.

Samples of notched specimen data were analyzed using equation (6) to calculate K_f, equation (5) to calculate e_a, equation (8) to calculate σ_{max}, and equation (3) to calculate e_{eq}. Optimum values of ρ for the K_f expression were found by using a computerized, iterative regression analysis analogous to that used in the m-parameter optimization on mean stress effects. Optimum ρ values are listed in table 5, along with the number of sample data.

TABLE 5. — OPTIMUM ρ VALUES DETERMINED IN NOTCHED FATIGUE ANALYSIS

Material	Optimum ρ, mm(in.)	Number of Data
2024-T3 Sheet	0.21(0.0083)	129
7075-T6 Sheet	0.17(0.0067)	130
300M Forging	0.046(0.0018)	191
Ti-6Al-4V Bar and Extrusion	0.020(0.0008)	53

The Relationship Between Fatigue
Life and Equivalent Strain

After adequate methods for consolidation of notched and unnotched fatigue data had been developed, it became of interest to analytically describe the consolidated data trends. Since stress (or strain) conditions and notch geometry are the controlled variables in most fatigue experiments, equivalent strain, which is based on these parameters, was considered the independent variable. Fatigue life was chosen as the dependent variable, since it is not controlled and generally displays an intrinsic variability.

TABLE 4. — CONSTANTS USED TO DEFINE MONOTONIC STRESS-STRAIN CURVES

Material[a]	$E,$ MN/m^2 (ksi)	$K_1,$ MN/m^2 (ksi)	$K_2,$ MN/m^2 (ksi)	$\sigma_a(1),$ MN/m^2 (ksi)	$\sigma_a(2),$ MN/m^2 (ksi)	$\epsilon_a(1)$	$\epsilon_a(2)$	n_1	n_2
2024-T4 Bar	70 300 (10 200)	841 (122)	462 (67)	274 (40)	379 (55)	0.0039	0.0185	0.200	0.048
2024-T3 Sheet	73 100 (10 600)	1013 ·(147)	431 (62.5)	344 (50)	364 (53)	0.0047	0.0060	0.200	0.032
7075-T6 Bar	74 000 (10 300)	1303 (189)	827 (120)	444 (62)	601 (87)	0.0060	0.0265	0.213	0.087
7075-T6 Sheet	72 400 (10 500)	3240 (470)	889 (129)	493 (72)	544 (79)	0.0069	0.0086	0.375	0.103
300M Billet	199 900 (29 000)	24 950 (3620)	7860 (1140)	1280 (186)	1590 (231)	0.0064	0.0093	0.588	0.342
Ti-6A1-4V Plate	110 300 (16 000)	4450 (645)	1050 (153)	750 (109)	875 (127)	0.0068	0.0101	0.354	0.032
Ti-6A1-4V Cylindrical Forging	115 100 (16 700)	5100 (740)	1075 (156)	760 (110)	886 (129)	0.0066	0.0100	0.380	0.047
Ti-6A1-4V Hot Rolled Bar	108 900 (15 800)	4120 (598)	1330 (193)	937 (136)	1010 (147)	0.0086	0.0120	0.318	0.056
Ti-6A1-4V Bar	110 300 (16 000)	2860 (415)	1340 (194)	1100 (160)	1170 (170)	0.0100	0.0119	0.202	0.030

[a]All data are from references as cited in table 3.

A variety of functions was reviewed in an effort to find a relatively simple analytical formulation that would describe fatigue data trends throughout the life range of interest — from 10^2 to 10^8 cycles to failure. An inverse-hyperbolic tangent function was used in the original analysis (refs. 3 and 20). Additional considerations revealed, however, that the inverse-hyperbolic tangent function was deficient in several respects. The function did reasonably represent fatigue data trends between 10^3 and 10^8 cycles to failure, but it did not accurately represent expected low-cycle fatigue data trends below 10^3 cycles to failure. Strain-controlled low-cycle fatigue data usually follow a power law relationship between total strain range and fatigue life (when the plastic strain range is much larger than the elastic strain range). The semi-logarithmic concave-downward shape of the inverse-hyperbolic tangent function in the region below 10^3 cycles was completely in contrast to these trends. An additional problem was encountered in usage of the inverse-hyperbolic tangent function when reasonable upper and lower function limits were necessary and no valid data were available in the high-cycle or low-cycle regions to provide an indication of true fatigue data trends in these areas.

An alternate formulation was developed to avoid some of the problems encountered in usage of the inverse-hyperbolic tangent equation. In its general form it is expressed as

$$N_f = B_1 \ \epsilon_{eq}^{m_1} + B_2 \ \epsilon_{eq}^{m_2}, \ B_1 \text{ and } B_2 \geq 0 \tag{9}$$

and essentially represents a universal-slopes-type relationship (ref. 21) in equivalent strain. The exponents, m_1 and m_2, are not equal to the inverse of the elastic and plastic slopes of a standard strain-range, fatigue-life plot as might first be suspected, but they are related to these parameters. The interrelationship of m_1 and m_2 to the universal-slopes-type parameters is illustrated in Appendix C. In this work, the exponents m_1 and m_2 were not from the universal-slopes expression, but were found through an iterative regression analysis.

The exponents m_1 and m_2 in equation (9) provide an indication of the sensitivity of fatigue life to changes in equivalent strain in the high- and low-cycle fatigue regions. This point is illustrated in figure 5 where a typical scatter band of unnotched fatigue data is shown. In the region from 10^2 to 10^5
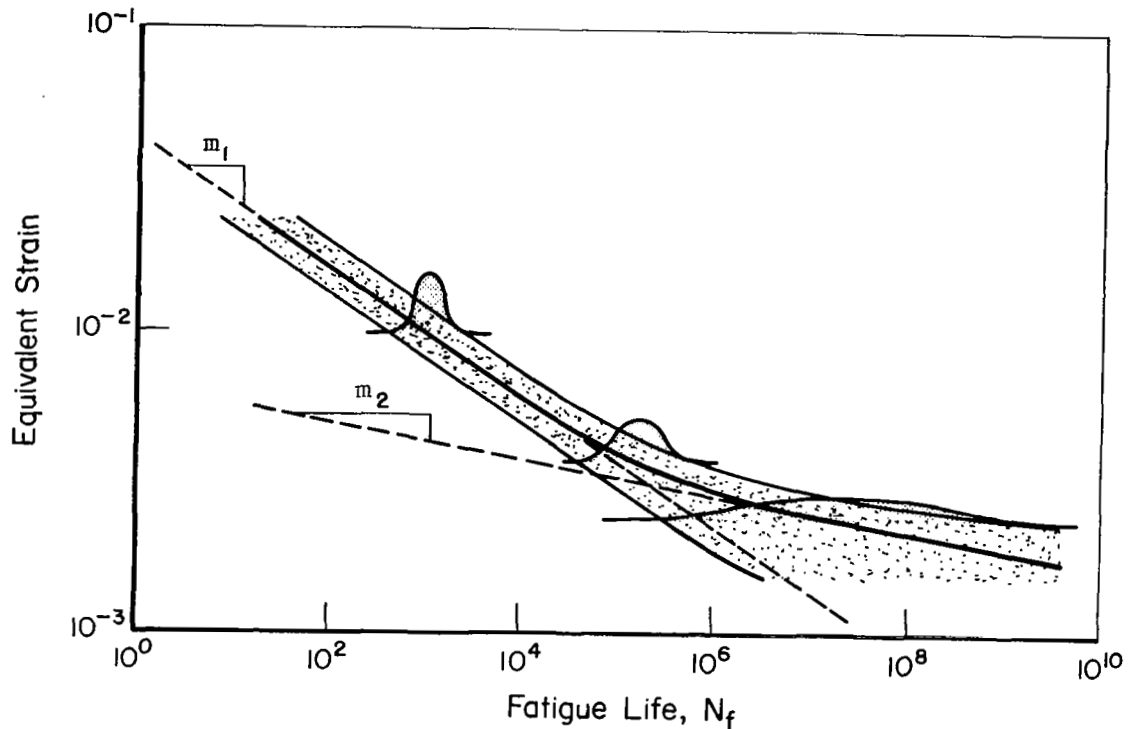
Figure 5. — Schematic illustration of typical fatigue data
trends in the region from 10^2 to 10^8 cycles to failure.

cycles, the sensitivity of fatigue life to variations in equivalent strain is usually constant and the variability in the data is relatively uniform (refs. 22 and 23). Beyond 10^5 cycles to failure, however, the sensitivity of fatigue life to decreased equivalent strains commonly increases along with the intrinsic data variability.

In some situations where limited data exist in the high-cycle regime, the available data at lower lives are best described by a simplified form of equation (9) as

$$N_f = B_1 \, \epsilon_{eq}^{m_1} \, , \, B_1 > 0 \tag{10}$$

Another consideration in this study, beyond development of mean fatigue life curves, was the construction of statistically based lower bounds on the consolidated fatigue data. These limits were to be calculated so as to define an interval which could be claimed to contain a specified proportion of the data population with a specific degree of confidence. Before these limits

24

could be calculated, it was necessary t⸱ etermine whether the data satisfied
the appropriate statistical conditions Primarily, the data had to be inde-
pendent, and log-normally distributed with zero mean deviations and constant
variance (ref. 24). Of these considerations, the uniformity of variance was
of greatest concern. As is illustrated in figure 5, the variability in fatigue
data commonly increases substantially beyond 10^5 cycles to failure.

To account for this problem, an empirically based weighting function was
devised which provided essentially uniform variances within the transformed
fatigue data. The weighting function was inherently quite reasonable because
it was determined on the basis of calculated sample estimates of variance at
various intervals of fatigue life. Figure 6 illustrates the method by which
the weighting function was established. Constant variance below 10^5 cycles was
calculated (and verified) by the sample estimates of variance. The rate of
increase in variance beyond 10^5 cycles was described analytically by a second-
order equation which was fitted to the sample estimates of variance. The
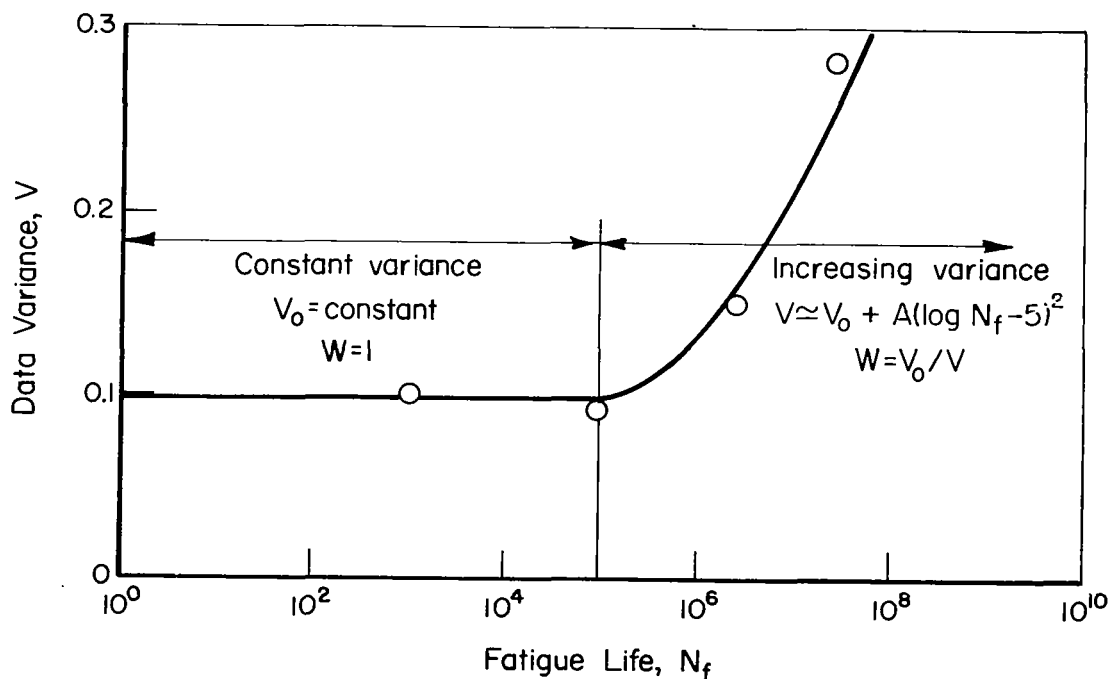
Figure 6. — Illustration of increasing variance for
$N_f > 10^5$ cycles and an approximate function
describing these trends.

weighting function was then analytically expressed as

$$W (\log N_f) = 1.0, \quad 0 < \log N_f \leq 5$$

$$W (\log N_f) = \frac{V_o}{V_o + A (\log N_f - 5)^2}, \quad \log N_f > 5 \tag{11}$$

Values of A were normally in the range of 0.08 to 0.15, but in several cases where scatter was quite large throughout the range of data, A was essentially zero, and the weighting of the data was uniform throughout.

Using equation (9) or (10) to describe the mean fatigue life trends, it was then possible to develop approximate lower bounds or tolerance limits on the consolidated fatigue data. Tolerance limits were calculated at discrete levels of equivalent strain according to the formulation

$$\log N_f = \log N_{f_{avg}} - \left(k_{u,\nu} s_{y \cdot x}\right)\Big/\sqrt{W(\log N_f)} \tag{12}$$

where $k_{u,\nu}$ represented a one-sided tolerance limit factor (ref. 25) for a normally distributed variable with $n - 2$ degrees of freedom. The subscripts u and ν describe the tolerance and confidence levels, respectively, while $s_{y \cdot x}$ represents the sample estimate of standard deviation for fatigue data with mean lives less than 10^5 cycles to failure. Log-normality of the data was not proven, but an examination of the residuals showed that this assumption was reasonable. Other research (refs. 22 and 23) also support this assumption.

Equation 12 should be used with care when developing tolerance limits at high fatigue lives (low equivalent strains). It is possible under these conditions, especially where only a small number of data or highly scattered data exist, that the tolerance level curve will begin to unrealistically decrease for decreasing equivalent strain (increasing fatigue life).

Results of Fatigue Analysis

Through the course of this program, a fatigue data consolidation and modeling process was developed through which a conglomerate set of fatigue test data at various mean stresses and notch concentrations could be

consolidated into a single curve and be reasonably described by a simple
analytical expression. Also, statistical considerations were applied, incor-
porating weight factors so that probability of survival curves could be
constructed below this consolidated data band.

This process was successfully applied to 2024 and 7075 aluminum alloys in
several different product forms and tempers and to 300M steel in the forged
condition. It was also used with reasonable success on Ti-6Al-4V alloy, con-
sisting of numerous product forms and heat-treatment conditions.

In these analyses, notched and unnotched-specimen data were treated
separately because combinations of the two data types resulted in substantial
increases in overall scatter. If a more realistic analysis of notch-root
stress-strain behavior had been available, the notched and unnotched data
possibly could have been treated jointly. At this point, however, it was
considered most useful to analyze notched and unnotched data separately,
especially since data samples were sufficiently large to allow consideration
of each subset on a statistical basis.

Table 6 summarizes the results of the analyses for all the available data
on the investigated materials. The number of data points are listed for each
set of data along with the standard deviation, the weight parameter A, and
the optimum coefficients and exponents for equations (9) or (10). The range
of applicability (which corresponds to the range of data) of the regressed
equation is listed in the final column for each data set. Graphic displays
of the consolidated data listed in table 6 are presented in figures 7 through
24. Each figure shows the consolidated data along with the regressed mean
curve and the calculated 90 and 99 percent statistical tolerance curves,
respectively, which were established at a 95-percent confidence level; the
curves are labeled in figure 7 so that it is easier to identify these lines.

The number of data points displayed in these plots differs in some cases
from the number presented in earlier reported work (ref. 3). This discrepancy
is due to two factors. First, some of the short-life unnotched data included
in earlier plots were load-control tests which displayed substantial plastic
strains. The validity of these data was questionable so all load-control
unnotched data with stable plastic strain amplitude greater than 0.0005 were

TABLE 6. — RESULTS OF NOTCHED AND UNNOTCHED FATIGUE DATA CONSOLIDATION

$$[N_f = B_1 \epsilon_{eq}^{m_1} + B_2 \epsilon_{eq}^{m_2}]$$

Material	Type of Data	Number of Data Points	Weighted R^a, percent	Logarithmic Standard Deviation, Average $N_f \leq 10^6$	Weight Parameter, A	Regression Coefficients		Optimum Exponents		Range of Equation Applicability, $\log(N_f)$
						B_1	B_2	m_1	m_2	
2024-T3 Sheet	Unnotched	119	97	0.209	0.147	1.04×10^{-8}	1.71×10^{-26}	-5.50	-13.0	2.8 - 7.0
	Notched	887	97	0.269	0.073	1.02×10^{-16}	--	-8.90	--	1.8 - 7.3
2024-T4 Bar and Rod	Unnotched	61	98	0.166	0.242	7.94×10^{-13}	--	-7.42	--	1.0 - 6.3
	Notched	114	89	0.306	0.110	9.83×10^{-13}	--	-7.56	--	3.0 - 6.7
7075-T6 Sheet	Unnotched	211	96	0.207	0.112	1.04×10^{-9}	7.02×10^{-32}	-6.00	-14.2	2.8 - 7.1
	Notched	695	96	0.197	0.108	7.65×10^{-14}	--	-8.11	--	2.0 - 7.2
7075-T6 Clad Sheet	Unnotched	369	98	0.124	0 033	5.92×10^{-7}	--	-4.56	--	3.3 - 6.1
7075-T6, -T651 Bar	Unnotched	137	78	0.383	0.098	9.03×10^{-8}	8.21×10^{-37}	-5.00	-16.0	3.4 - 6.5
	Notched	485	89	0.299	0.053	1.02×10^{-9}	7.13×10^{-35}	-6.00	-16.0	2.6 - 7.0
300M Billet and Forging	Unnotched	289	85	0.287	0.143	3.08×10^{-11}	--	-6.95	--	2.4 - 6.2
	Notched	218	82	0.287	0.134	5.74×10^{-7}	1.47×10^{-40}	-5.00	-18.0	3.1 - 6.3
Annealed Ti-6Al-4V Sheet[a]	Unnotched	67	81	0.493	0.00	1.45×10^{-23}	--	-13.1	--	3.7 - 6.8
Bar, Extrusion, and Casting[b]		188	48	0.647	0.018	2.73×10^{-10}	--	-6.75	--	4.3 - 6.9
Bar, Extrusion, and Forging[a]		277	82	0.284	0.119	1.16×10^{-17}	--	-9.98	--	3.9 - 6.8
Annealed Ti-6Al-4V Bar, Extrusion, and Casting[b]	Notched	297	79	0.360	0.107	3.60×10^{-13}	--	-8.33	--	3.6 - 6.8
Sheet, Bar, Extrusion, and Forging[a]		45	54	0.536	0.177	2.68×10^{-8}	--	-6.20	--	4.2 - 6.3
STA Ti-6Al-4V Sheet, Forging, Casting, and Plate[c]	Unnotched	147	86	0.301	0.151	1.83×10^{-10}	--	-6.91	--	2.9 - 6.5
STA Ti-6Al-4V Sheet, Casting, and Plate[c]	Notched	124	82	0.558	0.083	6.96×10^{-17}	--	-10.4	--	2.7 - 6.5

[a] Monotonic and cyclic stress-strain calculations were based on data from Ti-6Al-4V hot-rolled bar (see tables 3 and 4).

[b] Monotonic and cyclic stress-strain calculations were based on data from Ti-6Al-4V cylindrical forging (see tables 3 and 4).

[c] Monotonic and cyclic stress-strain calculations were based on data from Ti-6Al-4V bar (see tables 3 and 4).

excluded. Second, some of the titanium data were reorganized in an attempt to achieve better overall consolidations.

Figures 7 through 10 are for 2024-T3 and 2024-T4 aluminum; figures 11 through 15 are for 7075-T6 and 7075-T651 aluminum. For both series of aluminum, the data consolidation was substantial (the unnotched-specimen data displayed a slightly better consolidation than the notched-specimen data).

Results for 300M steel are presented in figures 16 and 17. The standard deviation of these data samples was greater than that found for the aluminum alloys, but the overall data collapse was considered good since the inherent data scatter for this alloy was quite large.

The Ti-6Al-4V alloy data, displayed in figures 18 through 24, were the most difficult to analyze and provided poorer results than the steel and aluminum alloys. The difficulties were due to two major factors. First, the titanium data file consisted of a large number of different product forms and heat treatments. Although an attempt was made to develop accurate monotonic and cyclic stress-strain data for each variation, only a rough approximation of these curves was possible in most cases. Second, the inherent scatter in most of the titanium data was great, making a consolidation effort difficult. The best results were found for the Ti-6Al-4V in the solution-treated and aged condition.
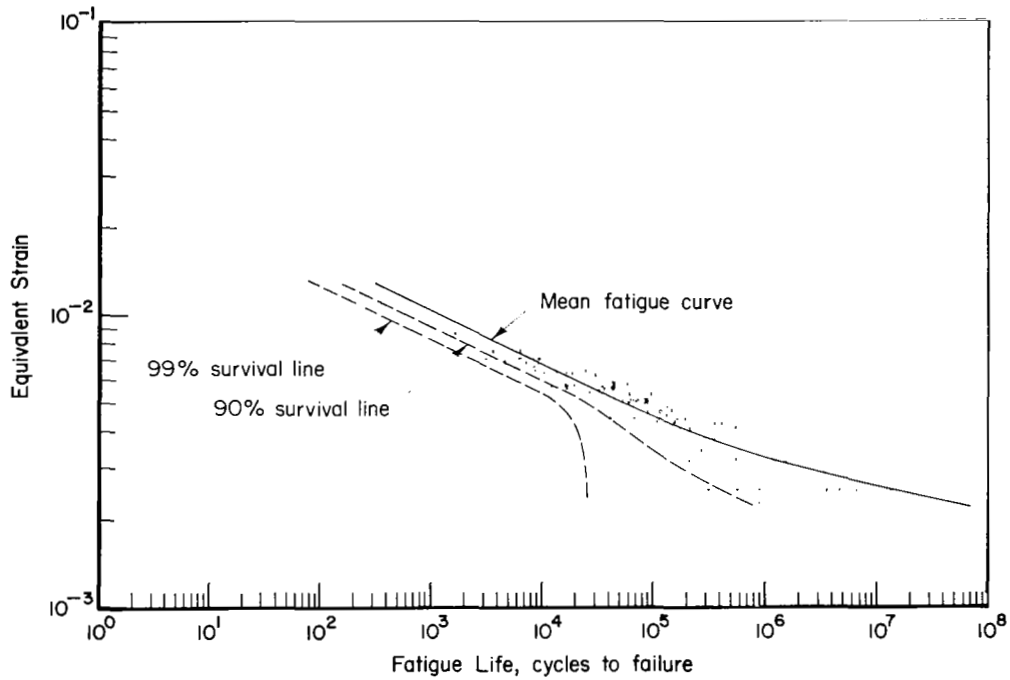
Figure 7. — Consolidated fatigue data, mean curve, and
tolerance limits for 2024-T3 sheet, unnotched.
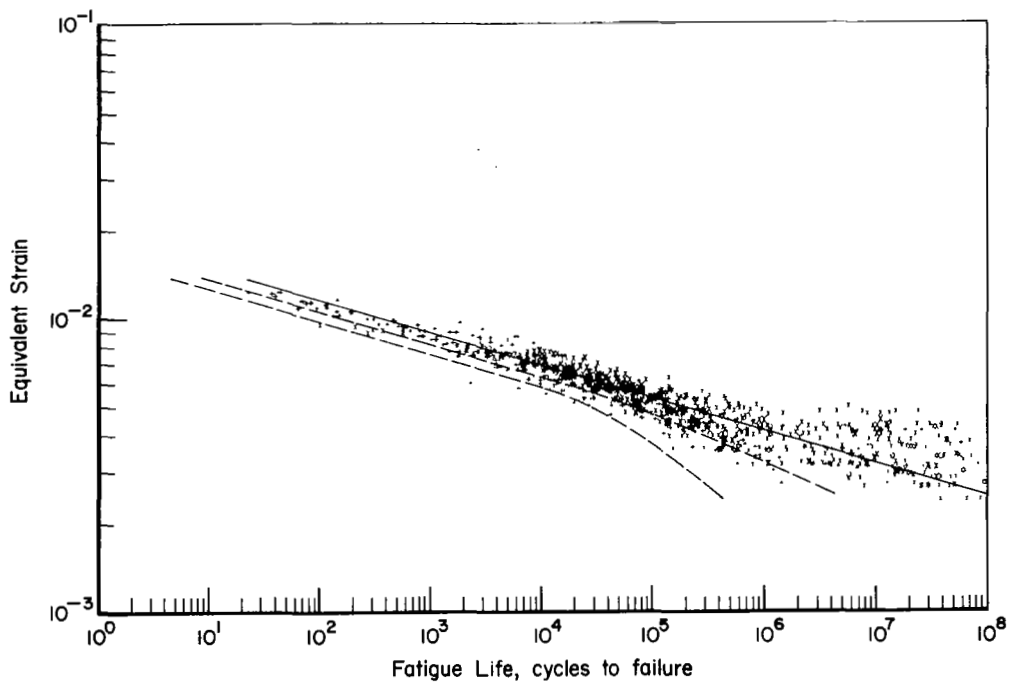
Figure 8. — Consolidated fatigue data, mean curve, and
tolerance limits for 2024-T3 sheet, notched.
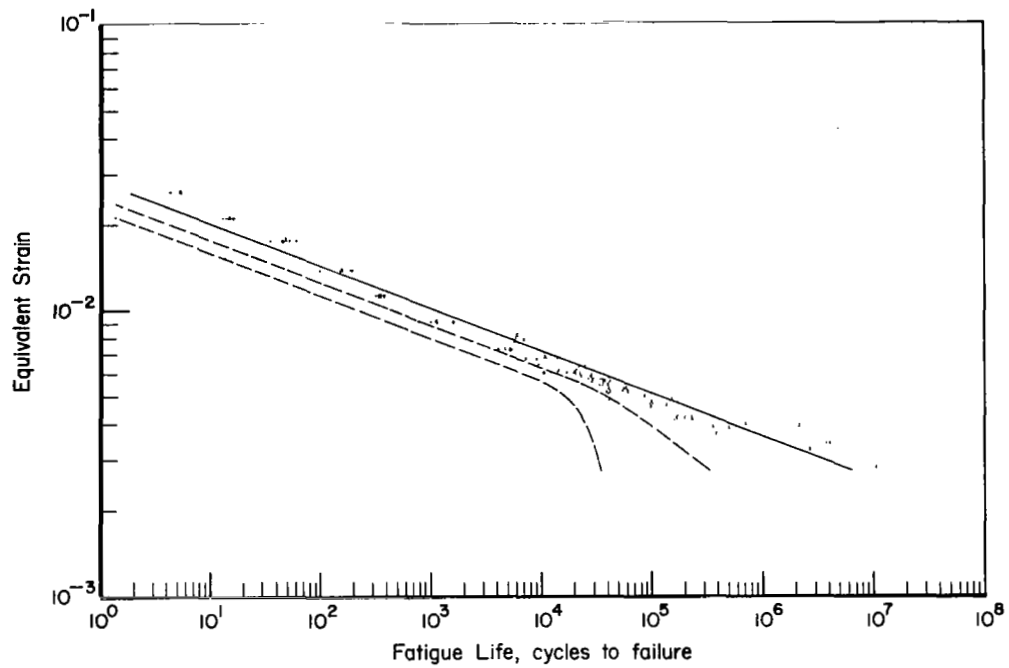
Figure 9. — Consolidated fatigue data, mean curve, and
tolerance limits for 2024-T4 bar and rod, unnotched.
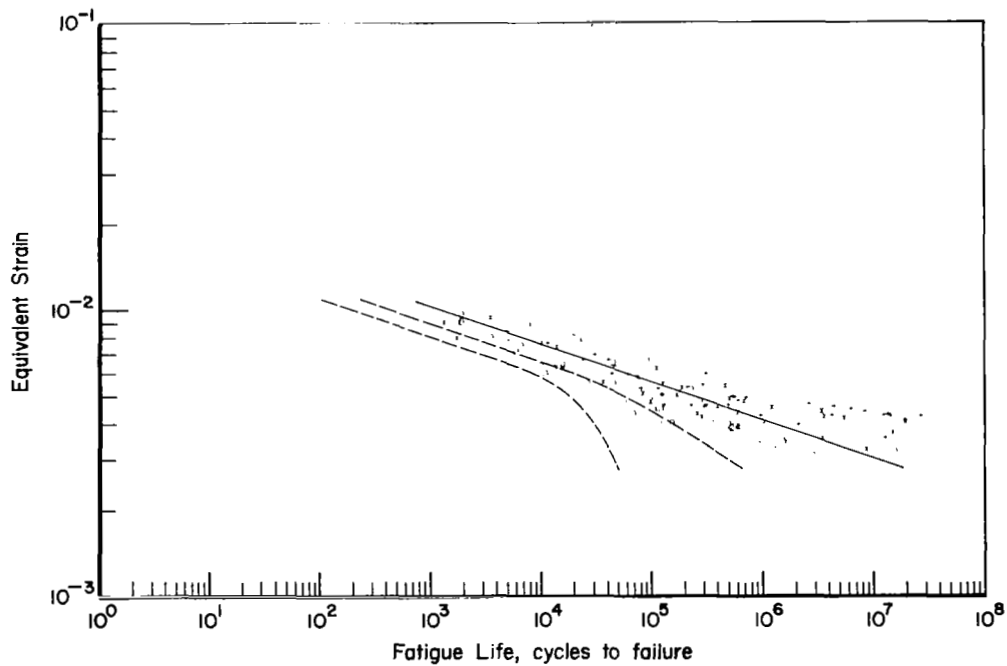
Figure 10. — Consolidated fatigue data, mean curve, and
tolerance limits for 2024-T4 bar and rod, notched.

31
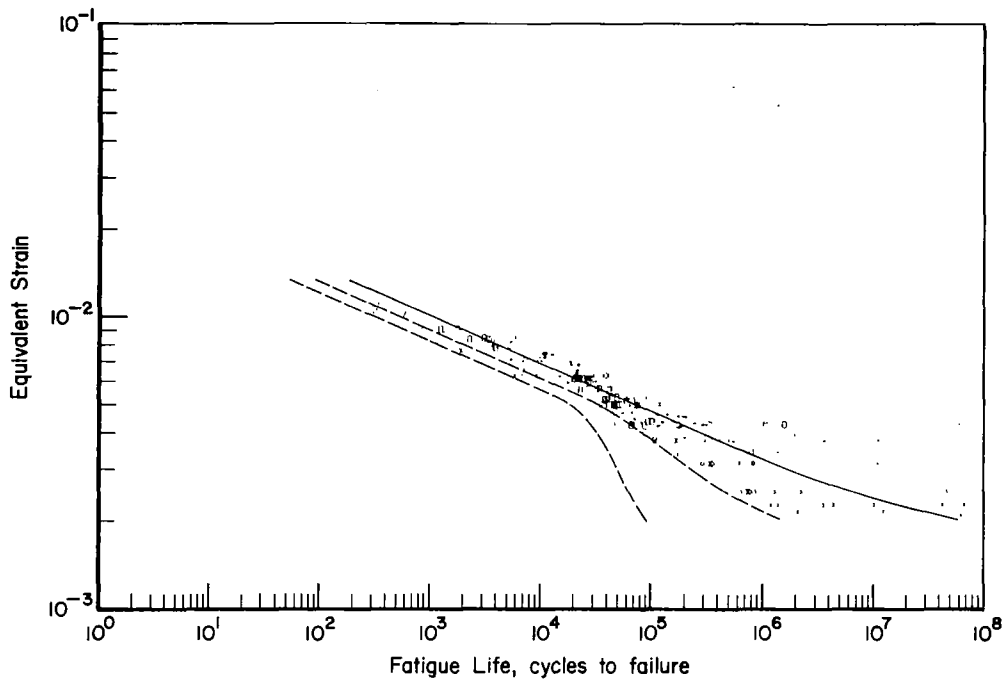
Figure 11. — Consolidated fatigue data, mean curve, and
tolerance limits for 7075-T6 sheet, unnotched.
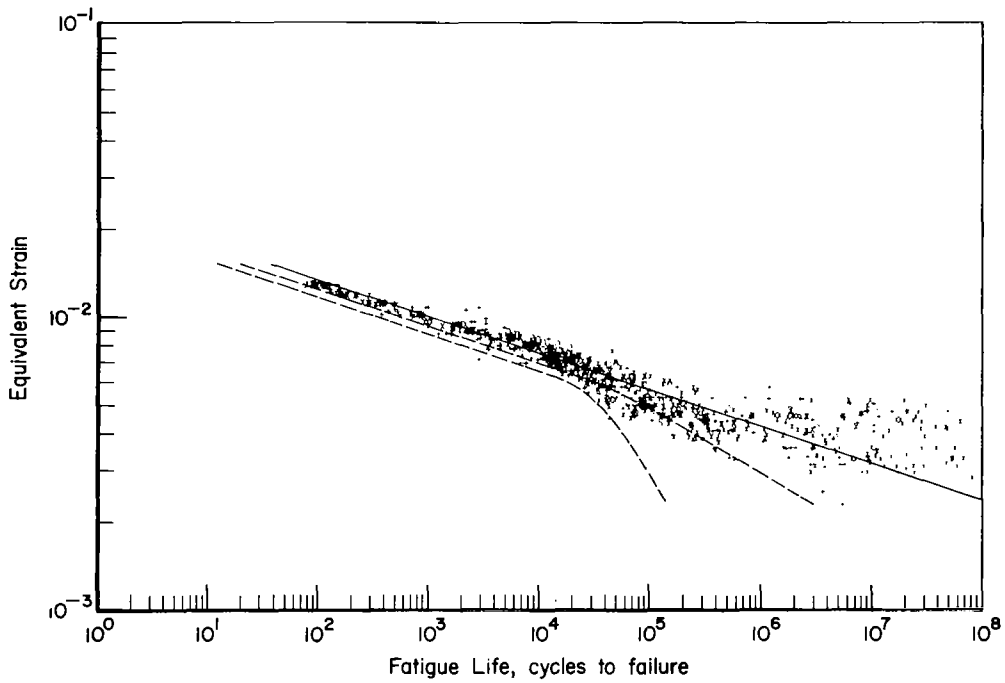
Figure 12. — Consolidated fatigue data, mean curve, and
tolerance limits for 7075-T6 sheet, notched.

32
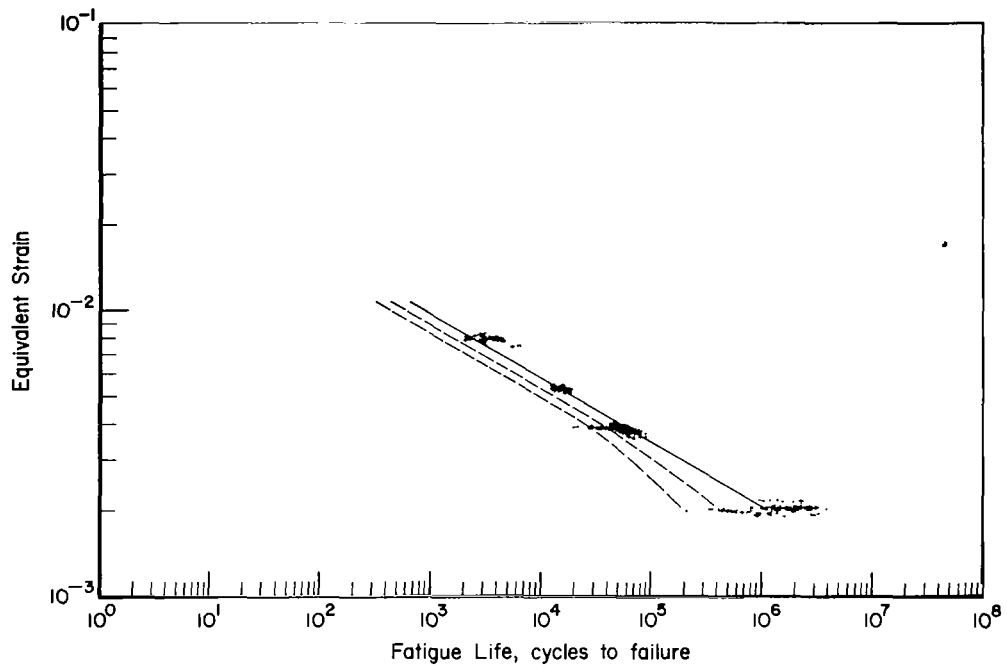
Figure 13. — Consolidated fatigue data, mean curve, and
tolerance limits for 7075-T6 clad sheet, unnotched.
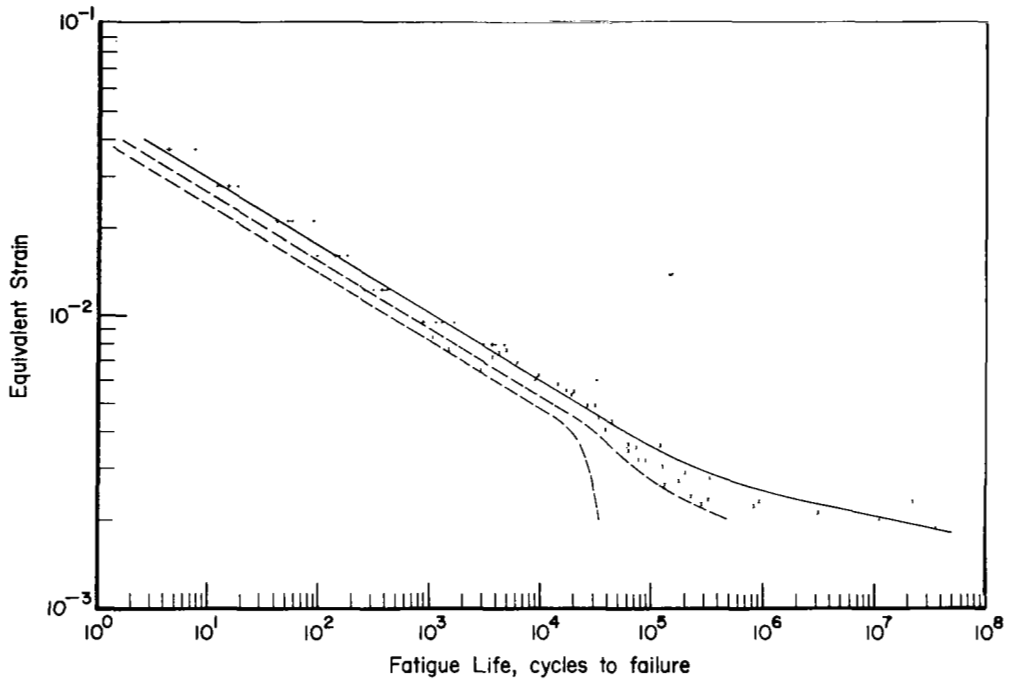
Figure 14. — Consolidated fatigue data, mean curve, and
tolerance limits for 7075-T6, -T651
aluminum bar, unnotched.
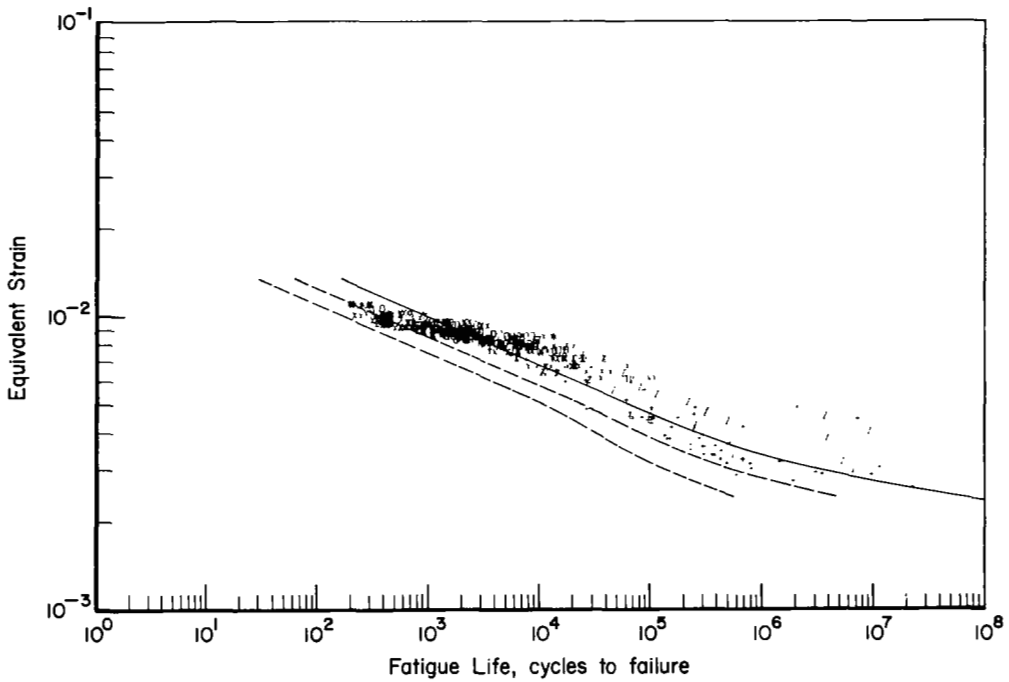
Figure 15. — Consolidated fatigue data, mean curve, and
tolerance limits for 7075-T6, -T651
aluminum bar, notched.
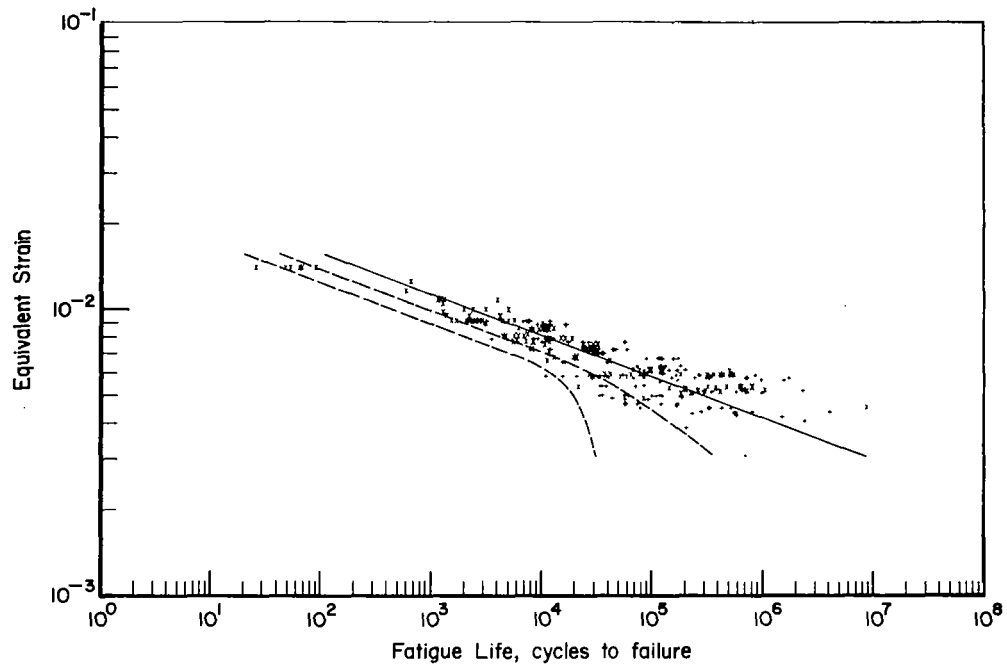
Figure 16. — Consolidated fatigue data, mean curve, and tolerance
limits for 300M forging and billet, unnotched.
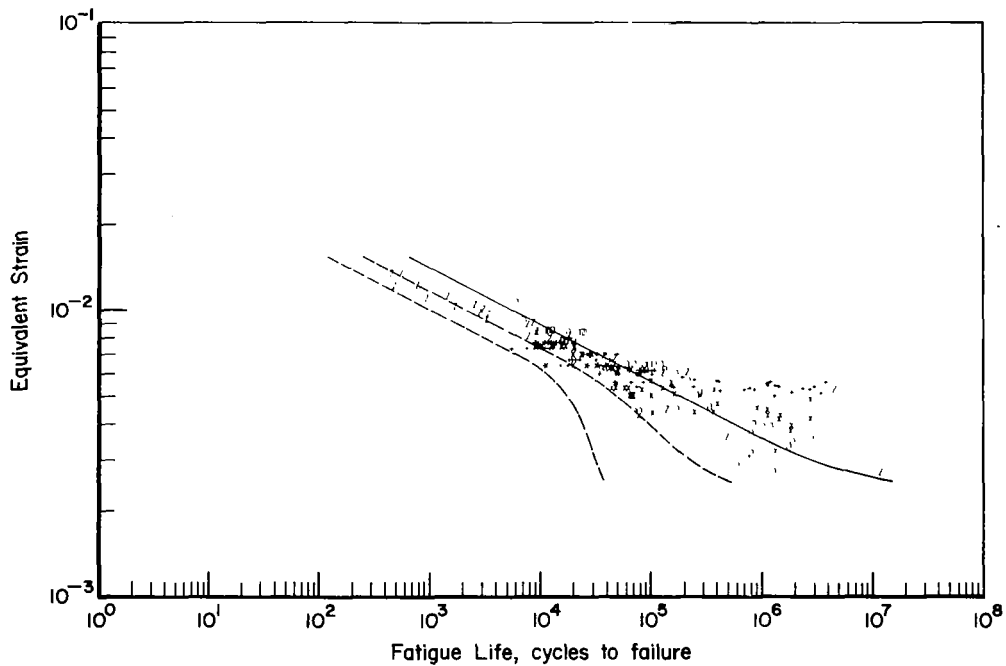
Figure 17. — Consolidated fatigue data, mean curve, and tolerance
limits for 300M forging and billet, notched.
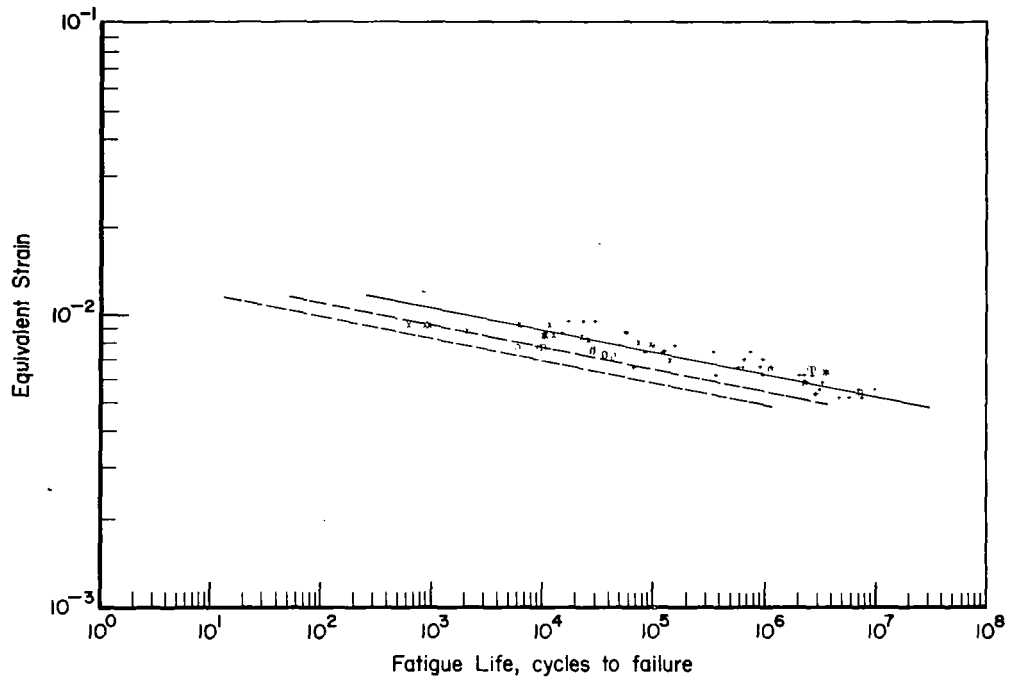
Figure 18. — Consolidated fatigue data, mean curve, and
tolerance limits for Ti-6Al-4V annealed sheet, unnotched.
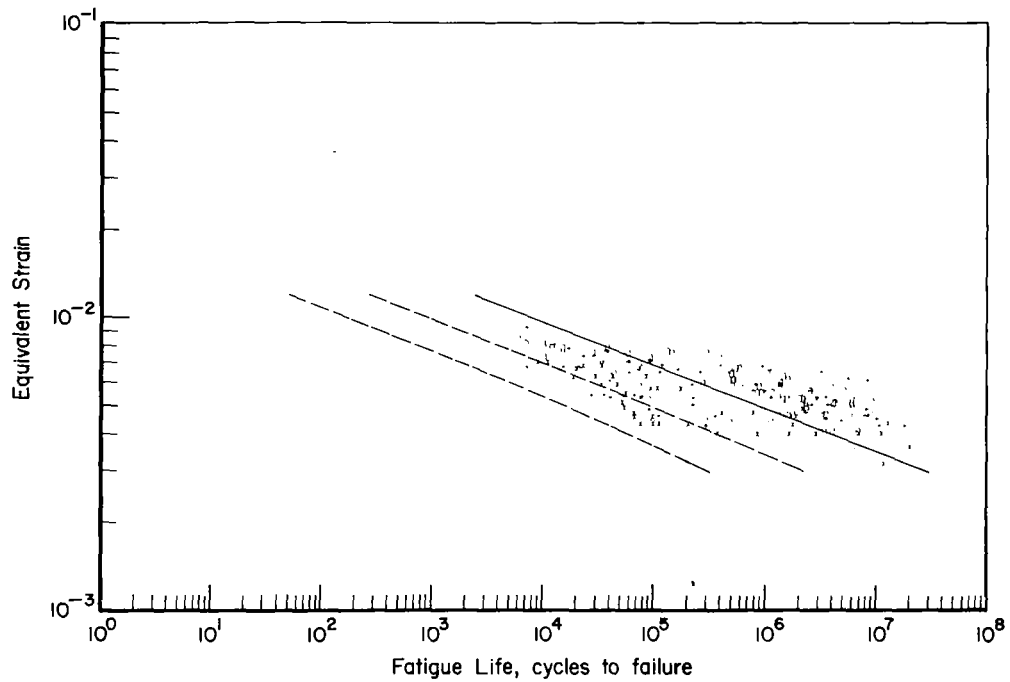
Figure 19. — Consolidated fatigue data, mean curve, and
tolerance limits for Ti-6Al-4V annealed
bar, extrusion, and casting, unnotched.
(See footnote "b" in table 6.)

36
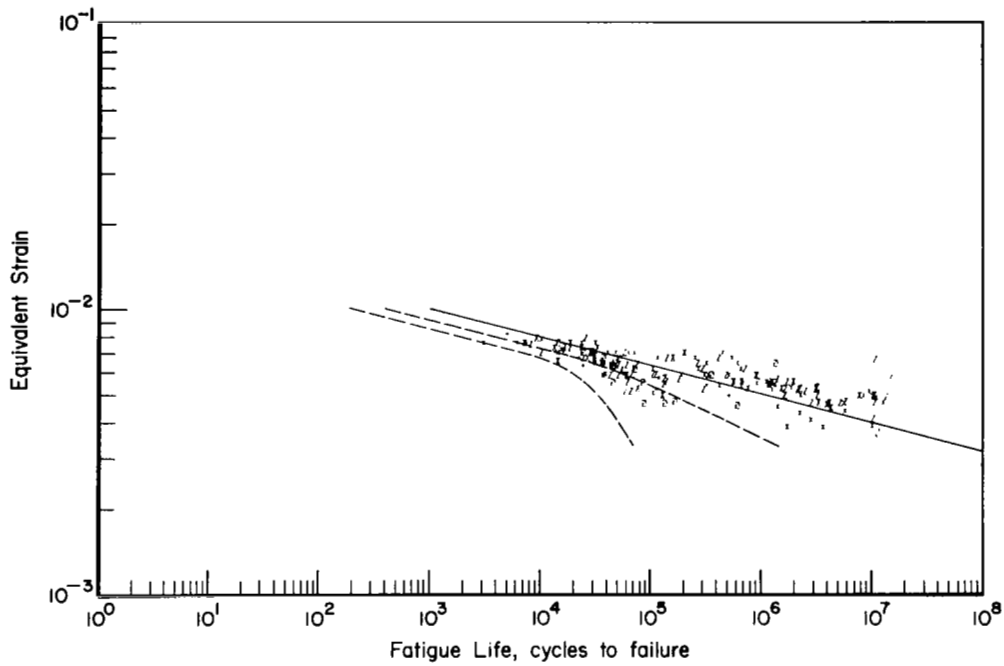
Figure 20. — Consolidated fatigue data, mean curve, and
tolerance limits for Ti-6A1-4V annealed bar,
extrusion, and forging, unnotched.
(See footnote "a" in table 6.)
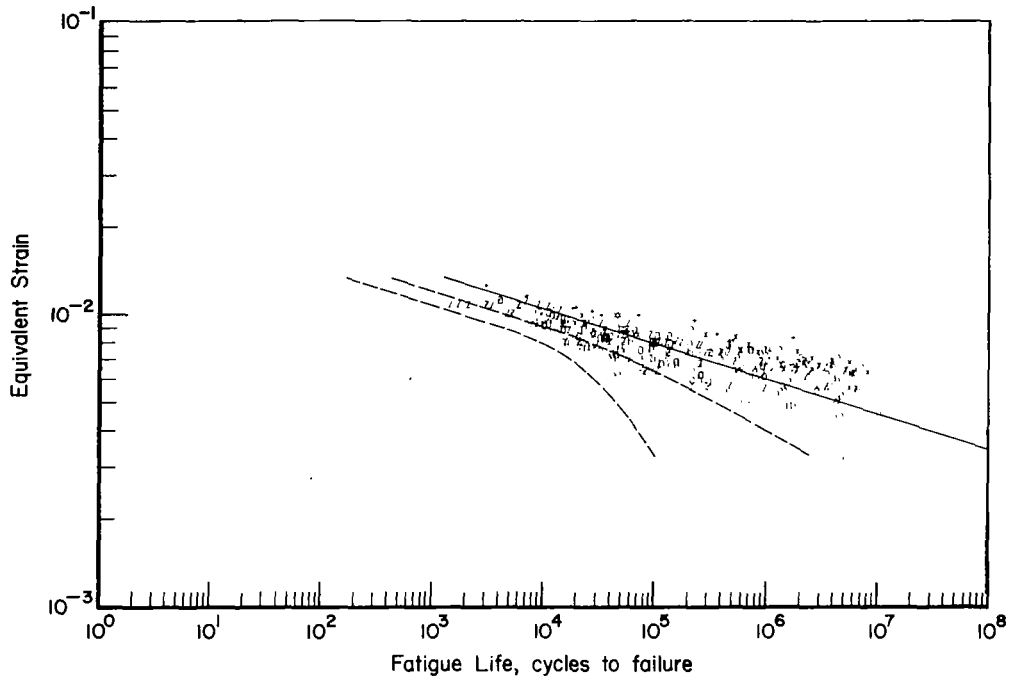
Figure 21. — Consolidated fatigue data, mean curve, and
tolerance limits for Ti-6Al-4V annealed bar,
extrusion, and casting, notched.
(See footnote "b" in table 6.)
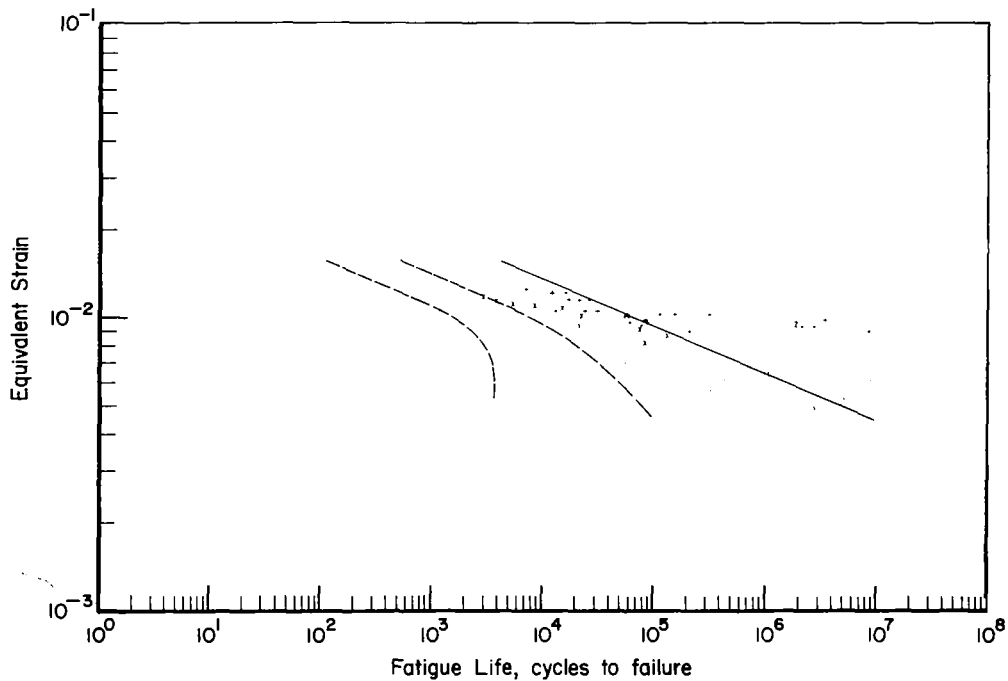
Figure 22. — Consolidated fatigue data, mean curve, and
tolerance limits for Ti-6Al-4V annealed sheet,
bar, extrusion, and forging, notched.
(See footnote "a" in table 6.)
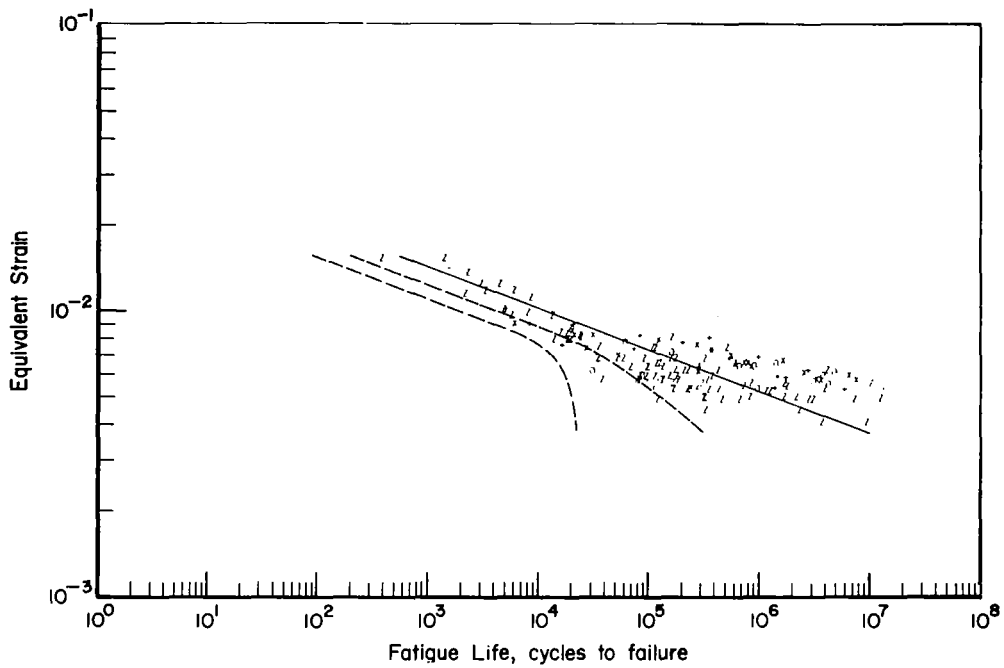
Figure 23. — Consolidated fatigue data, mean curve, and
tolerance limits for Ti-6Al-4V-STA sheet,
forging, casting, and plate, unnotched.
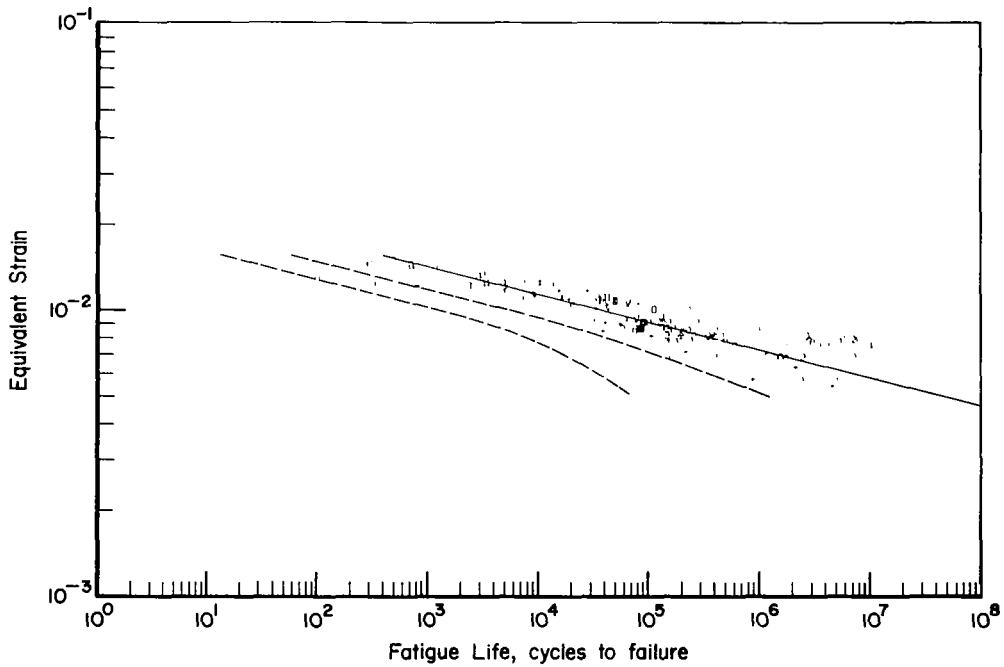
Figure 24. — Consolidated fatigue data, mean curve, and
tolerance limits for Ti-6Al-4V-STA sheet,
casting, and plate, notched.

Example of Fatigue Life Calculations

The following is a sample problem illustrating use of the concepts developed in this study for calculation of statistically based fatigue life estimates for constant-amplitude loading. The material and conditions were selected to represent a typical fatigue situation. Those conditions are listed below along with the known material parameters. The fatigue life estimates were calculated according to a five-step process, similar to that described in previous sections. Three estimates are calculated — a mean fatigue life value, a 90 percent survival value, and a 99 percent survival value.

Material and Conditions

Material	2024-T3 Sheet
Theoretical stress concentration	$K_t = 4.0$
Notch root radius	$r = 1.45$ mm (0.057 in.)
Stress ratio	$R = 0.2$
Maximum stress	$S_{max} = 172$ MN/m^2 (25.0 ksi)

Known Material Parameters

Equivalent strain material parameter	$m = 0.40$
Notch analysis material parameter	$\rho = 0.21$ mm (0.0083 in.)
Elastic modulus	$E = 73\ 100$ MN/m^2 (10 600 ksi)

Monotonic stress-strain parameters

$$K_1 = 1013 \text{ MN/m}^2 \text{ (147 ksi)}$$
$$K_2 = 431 \text{ MN/m}^2 \text{ (62.5 ksi)}$$
$$n_1 = 0.200$$
$$n_2 = 0.032$$
$$\epsilon_a(1) = 0.0047$$
$$\epsilon_a(2) = 0.0060$$
$$\sigma_a(1) = 344 \text{ MN/m}^2 \text{ (50 ksi)}$$
$$\sigma_a(2) = 364 \text{ MN/m}^2 \text{ (53 ksi)}$$

Cyclic stress-strain parameters

$$K_1 = 5135 \text{ MN/m}^2 \text{ (745 ksi)}$$
$$K_2 = 917 \text{ MN/m}^2 \text{ (133 ksi)}$$
$$n_1 = 0.499$$
$$n_2 = 0.150$$
$$\epsilon_a(1) = 0.0049$$
$$\epsilon_a(2) = 0.0071$$
$$\sigma_a(1) = 358 \text{ MN/m}^2 \text{ (52 ksi)}$$
$$\sigma_a(2) = 435 \text{ MN/m}^2 \text{ (63 ksi)}$$

Fatigue life
Equation
$$N_f = B_1 \, \epsilon_{eq}^{m_1},$$
where $B_1 = 1.02 \times 10^{-15}$
$m_1 = -8.90$

Standard deviation of data, $\quad s = 0.269$
$N_{f_{avg}} \leq 10^5$ cycles

Weight factor on data variability $\quad A = 0.073$

Step 1 — Compute K_f

$$K_f = 1 + \frac{K_t - 1}{1 + \rho/r}$$

$$= 3.62$$

Step 2 — Compute ϵ_a and ϵ_{max}

$$\epsilon_a = K_f \, e_a = K_f \, \frac{S_a}{E}$$

$$= \frac{K_f \, [S_{max} \, (1.0 - R)]}{2E}$$

$$= 5.12 \times 10^{-3}$$

$$\epsilon_{max} = K_f \, e_{max} = \frac{K_f \, S_{max}}{E}$$

$$= 8.54 \times 10^{-3}$$

Step 3 — Compute σ_{max}

$$\sigma_{max} = f_m(\epsilon_{max}) + [f_c(\epsilon_a) - f_m(\epsilon_a)]$$

$$= \left[K_2 (\epsilon_{max})^{m_2} \right]_m + \left[K_1 (\epsilon_a)^{m_1} \right]_c - \left[K_1 (\epsilon_a)^{m_1} \right]_m$$

$$= 386.5 \text{ MN/m}^2 \ (56.06 \text{ ksi})$$

Step 4 — Compute ϵ_{eq}

$$\epsilon_{eq} = (2\epsilon_a)^m \, (\sigma_{max}/E)^{1-m}$$

$$= 6.89 \times 10^{-3}$$

Step 5 — Compute N_f, $N_{f_{90}}$ and $N_{f_{99}}$

$$N_f = B_1 (\epsilon_{eq})^{m_1}$$

$$= 17 \ 720$$

$$\log N_{f_{90}} = \log N_f - k_{90,95} \, s_{y \cdot x}/1.0$$

$$= 4.248 - 0.369$$

$$N_{f_{90}} = 7570$$

$$\log N_{f_{99}} = \log N_f - k_{99,95} \, s_{y \cdot x}/1.0$$

$$= 4.248 - 0.662$$

$$N_{f_{99}} = 3855$$

This concludes the fatigue life calculations. It is worth noting that the 90 percent life calculated by this approach is slightly less than $\frac{1}{2}$ of the mean fatigue life and the 99 percent life is about $\frac{1}{4}$ of the mean.

FATIGUE-CRACK-PROPAGATION ANALYSIS

Extensive and varied laboratory studies have been conducted to characterize constant-amplitude fatigue-crack growth. Experimental data have been generated with a variety of specimen configurations, initial crack sizes, and environmental conditions. In general, the relationship between crack size and number of applied loading cycles is presented as a crack-growth curve drawn through the locus of experimentally derived data points. For a given material and initial crack size, families of crack-growth curves, parametric on maximum stress, stress ratio, and environment may be generated as these conditions are varied. In practice, fatigue-crack-propagation data in the basic form of crack-length measurements and cycle counts are not directly useful since, in addition to the above parameters, a variety of initial boundary conditions and geometric configurations are also encountered. To make a broader use of these data, they are generally interpreted in terms of rate behavior, $d(2a)/dN$, and expressed as some function of the stress-intensity factor

$$K = S\sqrt{\pi a} \; f(a,W) \tag{13}$$

in which $f(a,W)$ is a geometric scaling function dependent on crack size and shape and specimen geometry. Data converted to this form are usually plotted on logarithmic axes to obtain crack-growth rate curves for a given material.

The logarithmic plot of $d(2a)/dN$ versus K_{max} reveals a curve having a sigmoidal shape; rapidly decaying crack-growth rate is observed near the threshold of crack propagation and a rapidly increasing rate near the terminal point of stable crack growth. Within the general curve shape, systematic

variations in the data point locations are observed. For example, when data from tests conducted at several different stress ratios are present, the plot of crack-growth rate versus stress-intensity factor will be layered into bands about the locus of points having zero stress ratio. Layering of data points may also occur as a result of variation in other parameters such as test frequency, environment, and specimen grain direction.

It is particularly desirable to predict the characteristic effect of the stress ratio parameter. Assuming the variables K_{max}, R, and d(2a)/dN, the general form for the fatigue-crack-propagation model can be expressed as

$$\frac{d(2a)}{dN} = f(K_{max}, R) \tag{14}$$

The following subsections describe a useful method for characterizing and quantifying the fatigue-crack-growth-rate function. Methods of calculating crack-growth rates from laboratory data are discussed first. An approach to consolidating crack-growth-rate data is considered second. Then, a functional form for $f(K_{max}, R)$ is developed. Finally, the results of the application of this approach and an example of fatigue-crack-growth-rate calculation are presented.

Calculation of Crack-Growth Rates

In concept, the cyclic rate of fatigue-crack propagation, d(2a)/dN, is determined as the derivative (i.e., local slope) of the crack-growth curve (a versus N). However, in reality, since the crack-growth curve is known only from a point-wise, experimental sampling of the crack size at finite intervals of cycling, the growth rate must be inferred from an interpolation scheme based on the discrete samples of crack-growth measurements. Two general approaches exist for doing this. One approach is curve fitting wherein an analytical expression is fitted to all or part of the crack-growth data by least-squares regression techniques and, subsequently, differentiated to obtain the effective rate behavior. The other approach is incremental-slope approximation in which a slope-averaging technique is used in a local sense to define the rate behavior.

From the previous study (ref. 3) of several methods of rate calculation, it was concluded that a five-point (or fifth order) divided-difference scheme

provided the most suitable results in terms of an adequate fit of data without undue complexities of computational routines. This method consists of, first, considering the crack-growth data in sequential five-point subsets and then determining the crack-propagation rate at the midpoint of each subset as a weighted average of the four slope increments directly adjacent to (i.e., two increments preceding and two increments following) the midpoint. The nomenclature and conventions of this scheme are founded in numerical analysis and are an application of Newton's interpolation formula with divided differences (ref. 26). The computational procedure involves constructing sequential triangular arrays of divided differences and using these in the derivative of Newton's formula. For the ith five-point subset, the average rate (i.e., derivative of Newton's formula) at the midpoint, i + 2, may be expressed as

$$d(2a)/dN = f'(N_{i+2}) \approx f[N_i, N_{i+1}] + (2N_{i+2} - N_{i+1} - N_i) f[N_i, N_{i+1}, N_{i+2}]$$

$$+ (N_{i+2} - N_i)(N_{i+2} - N_{i+1}) f[N_i, N_{i+1}, N_{i+2}, N_{i+3}] \qquad (15)$$

$$+ (N_{i+2} - N_i)(N_{i+2} - N_{i+1})(N_{i+2} - N_{i+3}) f[N_i, N_{i+1}, N_{i+2}, N_{i+3}, N_{i+4}]$$

where $f[N_i, \ldots N_{i+k}]$ is the kth divided difference. This formulation is for the forward diagonal, which is one of several paths of equivalent accuracy that may be taken through the triangular array of differences. It was adopted and retained because it could be readily contracted or expanded for comparing other n-point groupings. Use of a divided-difference technique implies that a certain number of data points has to both precede and follow the data point at which the slope was being evaluated.

Consolidation of Crack-Growth-Rate Data Generated at Various Mean-Stress Levels

To account for the effects of stress ratio, and thus collapse data about the locus of points having R = 0, it was suggested that the independent variable be some function of K_{max} and R. As a general form for the independent variable, it was assumed that

$$K_{eff}(K_{max}, R) = U(R)K_{max} \qquad (16)$$

where U(R) was a functional relation to account for the effect of stress ratio.

A number of different forms for U(R) have been proposed. The study cited previously (ref. 3) presented the results of comparisons of several expressions. This comparison was made on the basis of application of the various equations to selected sets of fatigue-crack-propagation data. The expression yielding the best fit to the data was selected for the form of U(R). Of those relations compared, the expression proposed by Walker (ref. 4) produced the most satisfactory consolidation. Walker postulated that the independent variable should represent a combination of maximum stress-intensity factor and stress-intensity-factor range. Letting $U(R) = (1-R)^m$, K_{eff} becomes

$$K_{eff} = (1-R)^m K_{max} \tag{17}$$

where m is a coefficient to be optimized by an iterative procedure for each collection of data. Thus, the fatigue-crack-propagation data analyzed in this study were plotted and modeled in terms of $d(2a)/dN$ and K_{eff} as defined by equation (17).

Functional Relationship Between Crack-Growth Rate and Effective Stress-Intensity Factor

Numerous models of the type illustrated by equation (14) have been formulated by researchers during the last decade. Collections of proposed fatigue-crack-propagation models are presented in papers by Erdogan (ref. 27), Hoskin (ref. 28), and Coffin (ref. 29). Most of these are empirical relations designed to be fitted to crack-growth data by least-squares regression.

Having shown that considering crack-growth data in terms of crack-growth rate and effective stress-intensity factor resulted in good consolidation, it was necessary to select an appropriate functional relation between those variables. A fatigue-crack-propagation model was formulated that would fit the sigmoidal shape of the crack-growth-rate data. Collipriest (ref. 30) suggested that the inverse-hyperbolic-tangent function would provide a suitable curve shape. A fatigue-crack-propagation model was derived utilizing this functional form with K_{eff} as the independent variable. The resulting model was

$$\log \frac{d(2a)}{dN} = C_1 + C_2 \tanh^{-1} \left[\frac{\log[K_c K_o / (K_{max}(1-R)^m)^2]}{\log(K_o/K_c)} \right] \tag{18}$$

In this equation, C_1 and C_2 are regression coefficients to be determined by least-squares curve fitting. The asymptotic lower and upper limits of stable crack growth, K_o and K_c, on the K_{eff} axis, are selected either by inspection of the crack-growth-rate curve, plotted with K_{eff} as the abcissa, or by derivation from compilations of threshold and critical stress-intensity-factor values found in the literature. In the latter approach, K_c corresponds directly to a critical value presented in terms of K_{max}. K_o, on the other hand, corresponds to a threshold value presented in terms of K_{max} multiplied by $(1-R)^m$ where R is the largest value of stress ratio found in the crack-growth-rate data collection being analyzed. The selections made for K_o and K_c must be checked to verify that no values of K_{eff} for the data being analyzed lie outside those limits.

The inverse-hyperbolic-tangent model was compared with several commonly used fatigue-crack-propagation models by applying all of them to the analysis of selected sets of data (ref. 3). In all cases, equation (18) was found to give a better fit to the data; thus, it was selected for use.

Results of Fatigue-Crack-Propagation Analysis

A computer program was written to apply equation (18) to the analysis of fatigue-crack-propagation data. It performed the following analytical steps:

(1) Computed crack-propagation rates from the (a_i, N_i) pairs by equation (15).

(2) Calculated K_{max} values at each a_i for which a rate had been calculated by selecting the appropriate stress-intensity-factor formulation for the specimen geometry.

(3) Computed regression coefficients, C_1 and C_2 and optimized coefficient m by an iterative least-squares procedure. Iterated until the minimum sum of squares of the deviations was achieved.

(4) Calculated standard error of estimate and sum of squares of the deviations. Tolerance limits of 90 percent and 99 percent with 95 percent confidence were computed by the expression

$$\log \left.\frac{d(2a)}{dN}\right|_u = \log \frac{d(2a)}{dN} + s_{y \cdot x} k_{u,\nu} \tag{19}$$

(5) Printed out statistical parameters and regression coefficients. Plotted rate, $\left(\left.\frac{d(2a)}{dN}\right|_i, K_{eff_i}\right)$ data, the mean curve, and tolerance limits.

Extensive data sets on five materials were analyzed by the methods described. These materials were 7075-T6, 7075-T7351, and 2024-T3 aluminum alloys; 300M steel; and Ti-6Al-4V alloy. Fatigue-crack-growth-rate curves, resulting from the regression analysis are presented in figures 25 through 29. These plots show the experimental data, the mean curve, and the tolerance limits as plotted on logarithmic axes d(2a)/dN and K_{eff}. Table 7 presents a description of the data sets, regression and optimization coefficients, limits, and statistical parameters.

Good consolidation and representation of the data were obtained in most cases. Particularly satisfactory results were achieved for the titanium alloy.
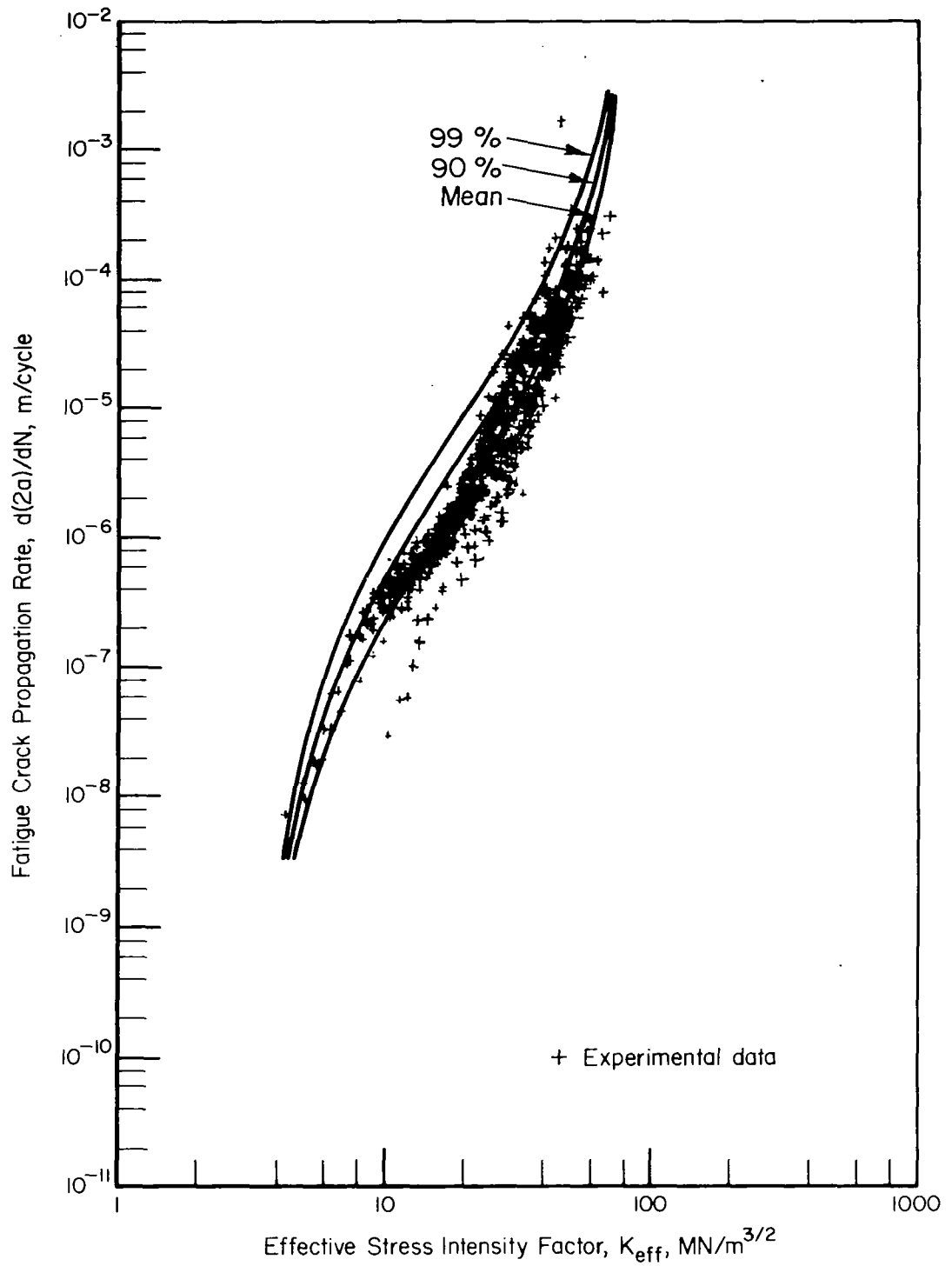
Figure 25. — Fatigue-crack-propagation-rate
curve for 7075-T6 alloy.
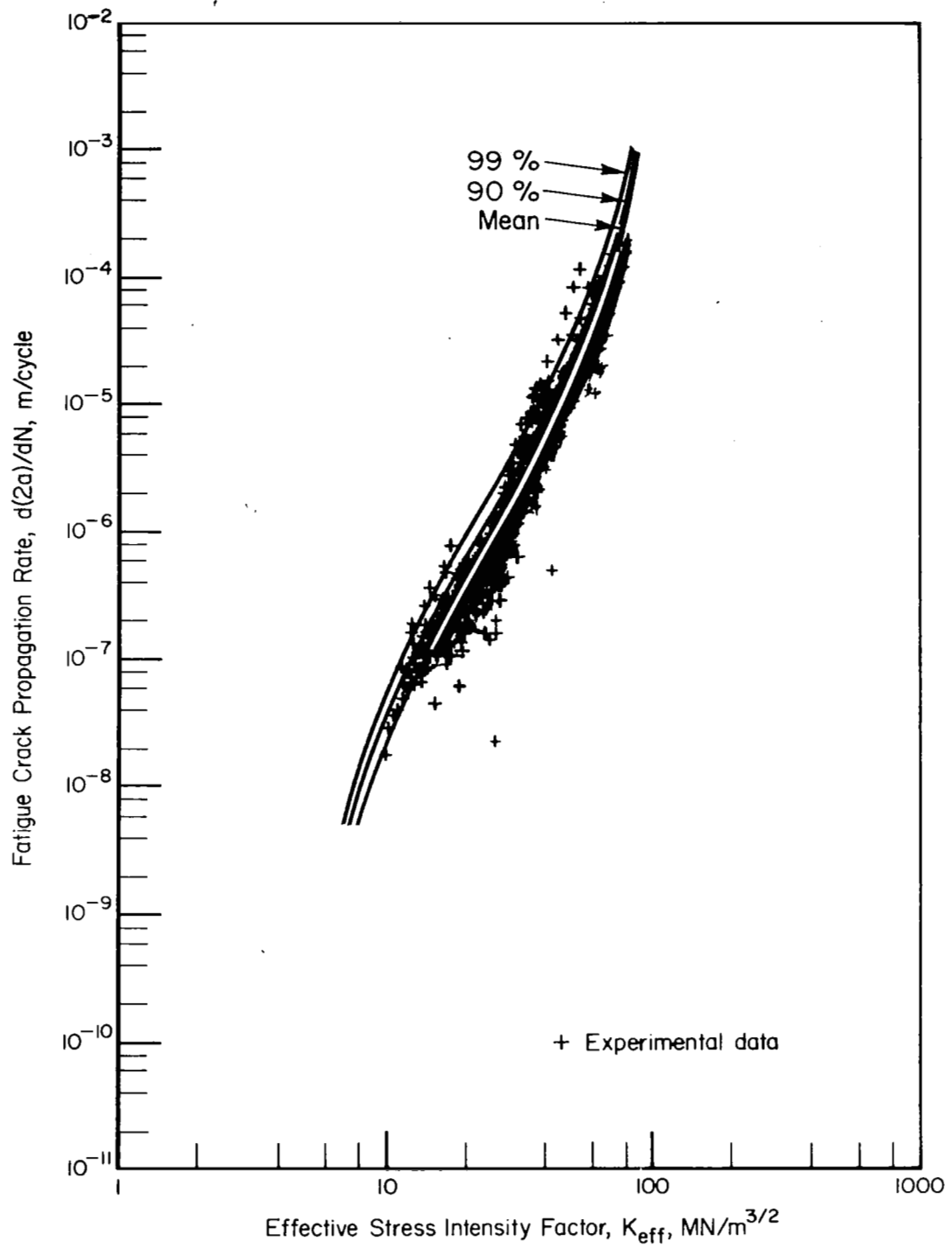
Figure 26. — Fatigue-crack-propagation-rate
curve for 7075-T7351 alloy.
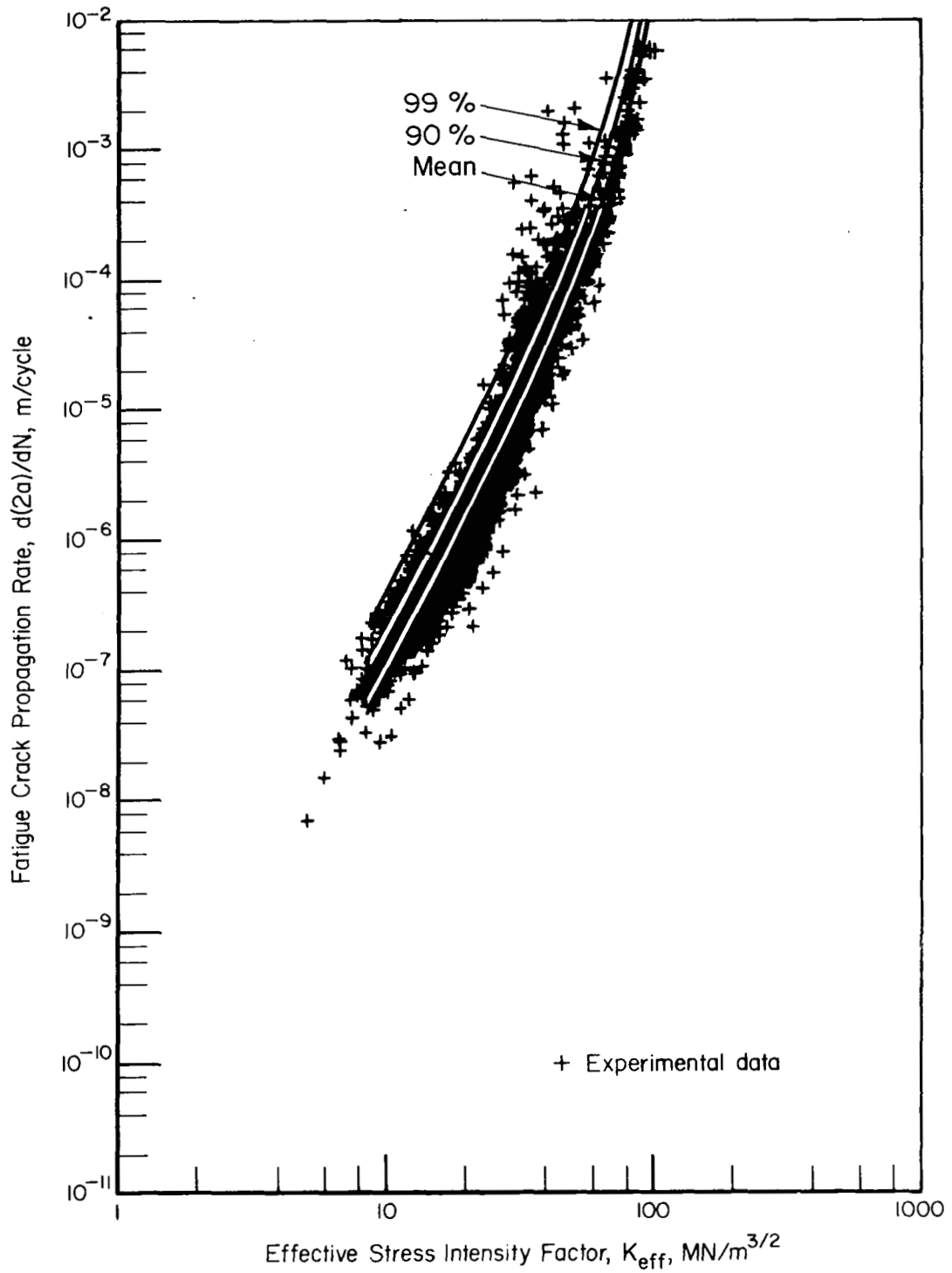
Figure 27. — Fatigue-crack-propagation-rate
curve for 2024-T3 alloy.
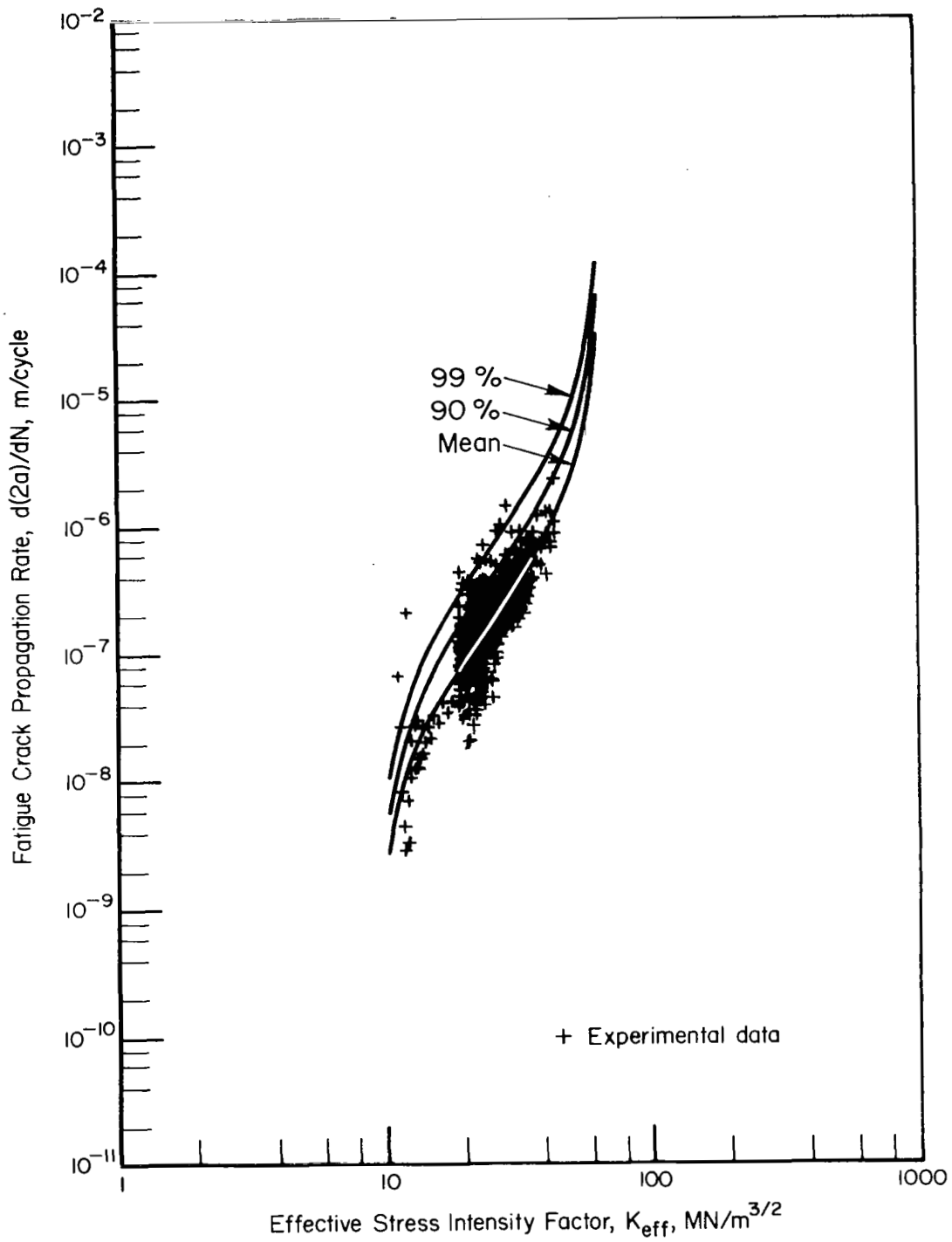
Figure 28. — Fatigue-crack-propagation-rate
curve for 300M steel.
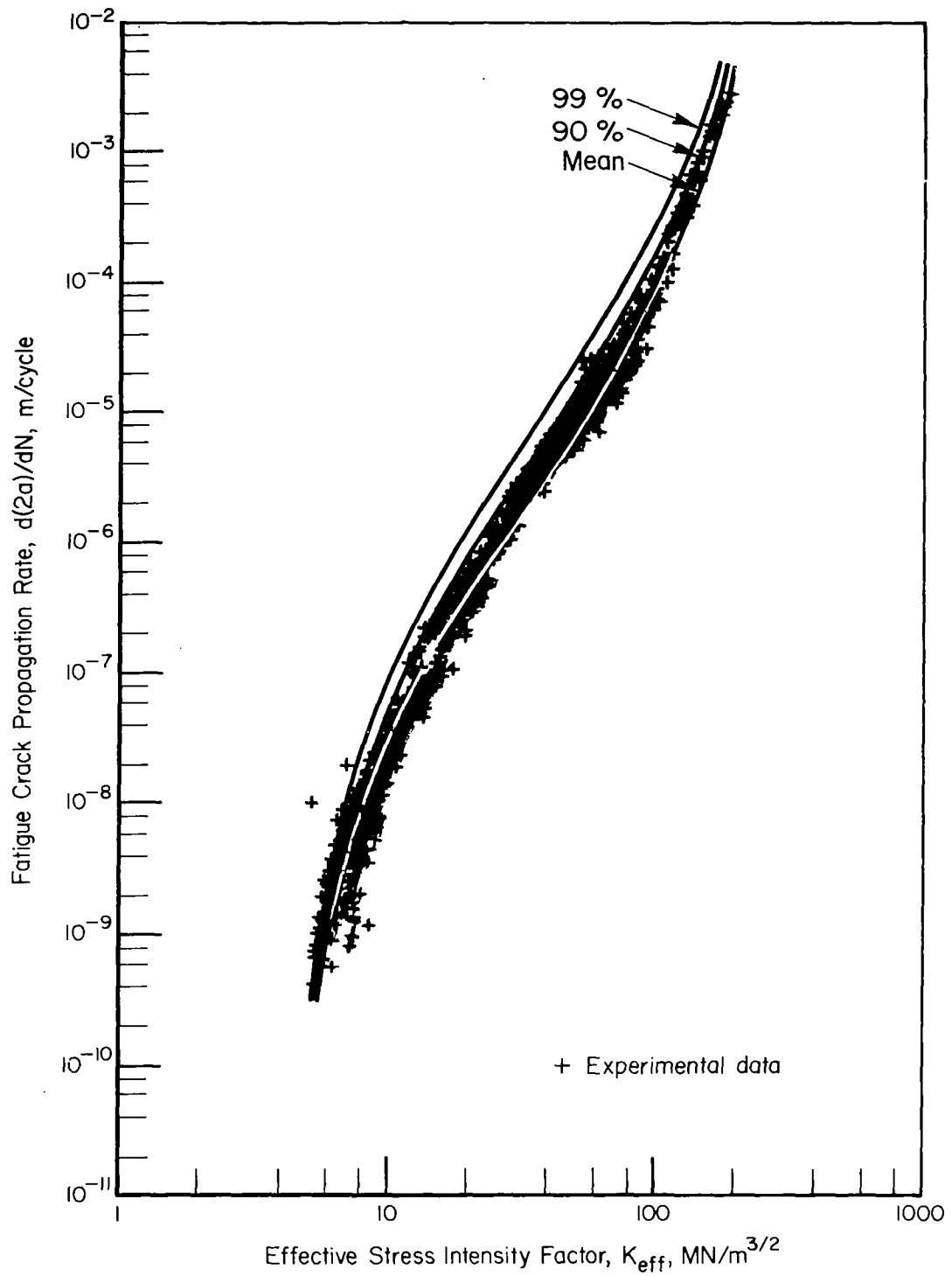
Figure 29. — Fatigue-crack-propagation-rate
curve for Ti-6Al-4V alloy.

TABLE 7. — CRACK-PROPAGATION DATA CONSOLIDATION

$$\log \frac{d(2a)}{dN} = C_1 + C_2 \tanh^{-1}\left[\frac{\log[K_c K_o/(K_{max}(1-R)^m)^2]}{\log(K_o/K_c)}\right]$$

Material	Specimen Types[a]	Number of Data Points, n	R^2	Standard Error of Estimates, $s_{y \cdot x}$	Regression Coefficients[b]		Optimized Coefficients, m	K_o, MN/m$^{3/2}$ (ksi-in.$^{1/2}$)	K_c, MN/m$^{3/2}$ (ksi-in.$^{1/2}$)
					C_1	C_2			
2024-T3 Bare and Clad Sheet and Plate	CC	3407	0.923	0.255	-4.490	3.465	0.420	2.20 (2.00)	142.74 (130.00)
7075-T6 Bare and Clad Sheet and Plate	CC	746	0.912	0.252	-4.207	2.241	0.320	3.29 (3.00)	85.64 (78.00)
7075-T7351 Bare Sheet and Plate	CC	1082	0.952	0.177	-4.043	2.574	0.350	4.36 (4.00)	109.90 (100.00)
300M Plate	CC	513	0.661	0.236	-5.186	1.296	0.335	8.78 (8.00)	65.88 (60.00)
Ti-6Al-4V Sheet and Forging	CC, CT	782	0.982	0.215	-4.046	2.825	0.580	4.39 (4.00)	274.50 (250.00)

[a] CC = center-cracked specimen; CT = compact-tension specimen.

[b] Regression coefficients C_1 and C_2 were derived from data in terms of customary units. Convert resulting data to SI units (m/cycle) by multiplying rate by 0.0254 m/in.

Example of Fatigue-Crack-Growth-Rate Calculation

The application of the crack-growth rate model, equation (18), is now illustrated by an example for a center-cracked panel. Suppose that it is wished to know the crack-growth rate when a crack is 0.014 m (0.543 in.) long in a 0.244 m (9.62 in.) wide Ti-6Al-4V panel. The panel is to be cyclically loaded to a maximum stress level of 206.8 MN/m^2 (30.0 ksi) with R = 0.70.

The procedure to be used is as follows:

Step 1 — Select the appropriate data for Ti-6Al-4V from table 7. Thus,

$$C_1 = -4.046$$
$$C_2 = 2.825$$
$$m = 0.580$$
$$n = 782$$
$$K_c = 274.50 \text{ MN/m}^{3/2}$$
$$K_o = 4.39 \text{ MN/m}^{3/2}$$
$$s_{y \cdot x} = 0.215$$

Step 2 — For the center-cracked panel assume that

$$K_{max} = S \sqrt{\pi a \sec\left(\frac{\pi a}{W}\right)} \qquad (19)$$

Using this relation, the maximum stress-intensity factor is found to be

$$K_{max} = 30.4 \text{ MN/m}^{3/2} \quad (27.7 \text{ ksi-in.}^{\frac{1}{2}})$$

Step 3 — Using equation (18), the crack-growth rate is given by

$$\log \frac{d(2a)}{dN} = -4.046 + 2.825 \tanh^{-1}\{\log[(274.5 \times 4.39)/$$
$$((30.4)(1-0.70)^{.58})^2]/\log[4.39/274.5]\} + \log(0.0254)$$

so that

$$\frac{d(2a)}{dN} = 1.44 \times 10^{-7} \text{ m/cycle} \quad (5.67 \times 10^{-6} \text{ in./cycle})$$

Step 4 — Tolerance limits may be established on the calculated growth rates by using equation (19). The 99 percent tolerance limit on rate, corresponding to $k_{u,\nu} = 2.445$ for 782 data points, is

$$\log \frac{d(2a)}{dN}\bigg|_{99} = -6.842 + (0.215)(2.445)$$

so that,

$$\frac{d(2a)}{dN}\bigg|_{99} = 4.83 \times 10^{-7} \text{ m/cycle} \quad (1.90 \times 10^{-5} \text{ in./cycle})$$

CONCLUSIONS

As a result of this study, it was found that large amounts of fatigue and fatigue-crack-propagation data can be consolidated for use in design applications. These two areas of material behavior were treated separately, using large files of pertinent data that were gathered on 2024 and 7075 aluminum alloys, Ti-6Al-4V alloy, and 300M steel. The analyses were limited to constant-amplitude cycling conditions.

From studies of fatigue data, it was concluded that

(1) An equivalent strain parameter can be used to account for effects of mean stress or stress ratio.

(2) A local stress-strain analysis, which uses an empirically computed K_f value and a technique to approximately account for cyclic stabilization of mean stress, can be used to account for notch effects.

(3) Fatigue life can be related to equivalent strain using a two-part power function.

(4) Using the two-part power function, it is possible to compute mean fatigue curves and one-sided tolerance limit curves for 90 and 99 percent probability of survival with 95 percent level of confidence.

From studies of fatigue-crack-propagation data, it was concluded that

(1) Crack-growth curves can be simply and effectively approximated using a five-point, divided-difference scheme.

(2) The Walker effective stress-intensity formulation can be used to account for stress-ratio effects.

(3) The inverse hyperbolic-tangent ($\tanh^{-1}$) function can be used to model crack-growth-rate curves.

(4) Using the $\tanh^{-1}$ function, mean growth rate curves and one-sided tolerance limit curves for 90 and 99 percent probability of maximum crack-growth rate with 95 percent confidence level can be developed.

APPENDIX A

CYCLIC STRESS-STRAIN DATA

The method of fatigue analysis developed in this program required the use of both cyclic and monotonic stress-strain curves. Using information from MIL-HDBK-5B (ref. 1), it was possible to characterize the monotonic stress-strain response for the materials of interest. However, outside of the data reported by Endo and Morrow (ref. 7), Landgraf, et al (ref. 8), Smith, et al (ref. 10), and Gamble (ref. 9), there was no appropriate information available on the cyclic stress-strain response of these same materials. To fill this void of information, a limited amount of complementary tests were conducted on 2.29 mm (0.09 in.) thick 2024-T3 and 7075-T6 aluminum sheet.

All specimens were axially loaded using an electrohydraulic test system operated in closed-loop strain control at a constant strain rate of 4×10^{-3} sec^{-1}. Experimental procedures were similar to those reported by Jaske, et al (ref. 31). Special lateral guides were used to prevent buckling. These guides were clamped about the specimen with a force light enough to avoid significantly influencing loading of the specimen. Strain was measured over a 12.7 mm (0.500 in.) gage length using a special extensometer with a linear variable displacement transformer (LVDT) as the transducer. Load was measured by a standard load cell in series with the specimen and continuously recorded on a time-based chart. Load-strain records were made periodically using an X-Y recorder.

Results of these experiments are summarized in table A1. For each alloy, three incremental step tests (ref. 8) were used to develop continuous monotonic and cyclic stress-strain curves up to 0.01 maximum strain (see figs. A1 and A2). To see if the cyclic stress-strain curves from the step tests could be used to predict cyclic stress-strain response under constant-amplitude strain cycling, seven specimens of each alloy were tested under constant-amplitude loading. For three tests the strain ratio (algebraic ratio of minimum to maximum strain) was equal to -1.0 (i.e., the mean strain was zero). A positive value of mean strain was used in the other four tests — three were with a strain ratio of 0.0 and one was at a strain ratio of 0.5.

In all cases, results from the constant-amplitude tests were close to those predicted by the cyclic stress-strain curve from the step tests (figs. A1 and A2). Thus, it was concluded that these cyclic stress-strain curves could be used to describe the stable stress-strain response of these two materials.

Cyclic stress-strain data were also generated on 300M steel and annealed Ti-6Al-4V alloy. Experimental procedures were the same as those described earlier, except that a 6.35 mm (0.250 in.) diameter, 12.7 mm (0.500 in.) gage length specimen was used. Cyclic stress-strain curves for these two alloys are presented in figures A3 and A4. Samples of the titanium alloy from the transverse (T) direction and from electron-beam (EB) welded plate cyclically hardened, whereas samples from the longitudinal (L) direction cyclically softened. The cyclic curve shown in figure A4 is for the L direction and the monotonic curve was estimated from published data (ref. 1). To show the wide variation in cyclic stress-strain behavior of this alloy, data from Smith, et al (ref. 10) are presented in figure A5 and data from Gamble (ref. 9) are presented in figures A6 and A7.

TABLE A1. — RESULTS OF CYCLIC STRESS-STRAIN TESTS AT A STRAIN RATE OF 4×10^{-3} SEC^{-1}

Specimen	Type of Test[a]	Strain Ratio[b]	Stable Strain Range		Stable Stress Range, $\Delta\sigma$, MN/m² (ksi)	Stable Mean Stress, σ_m, MN/m² (ksi)	Fatigue Life N_f, cycles[c] (or blocks)
			Total, $\Delta\varepsilon$	Plastic, $\Delta\varepsilon_p$			
2024-T3 Sheet							
2	STEP	-1.0	0.0204 max		--	--	23-1/40
3	STEP	-1.0	0.0204 max		--	--	17-2/40
4	STEP	-1.0	0.0200 max		--	--	19-39/40
1	CA	-1.0	0.0233	0.0105	938 (136)	--	324
9	CA	-1.0	0.0152	0.0029	917 (133)	--	756
5	CA	-1.0	0.0098	0.0005	745 (108)	--	6 140
7	CA	0	0.0206	0.0075	917 (133)	23 (3.4)	178
8	CA	0	0.0153	0.0029	917 (133)	7.6 (1.1)	1 137
6	CA	0	0.0101	0.0001	710 (103)	15 (2.2)	6 270
10	CA	0.5	0.0100	0.0002	717 (104)	36 (5.2)	4 260
7075-T6 Sheet							
1	STEP	-1.0	0.0208 max		--	--	28-5/40
2	STEP	-1.0	0.0204 max		--	--	34
3	STEP	-1.0	0.0206 max		--	--	30-37/40
6	CA	-1.0	0.0201	0.0056	1 050 (152)	--	292
10	CA	-1.0	0.0150	0.0011	944 (137)	--	1 209
4	CA	-1.0	0.0097	0.0001	710 (103)	--	6 173
8	CA	0	0.0204	0.0050	1 000 (145)	49 (7.1)	270
9	CA	0	0.0152	0.0007	979 (142)	43 (6.3)	511
7	CA	0	0.0101	--	703 (102)	160 (23.2)	4 611
11	CA	0.5	0.0096	--	684 (99.2)	198 (28.2)	3 270

[a]STEP indicates an incremental step test and CA indicates a constant-amplitude test.

[b]Ratio of minimum to maximum strain.

[c]Cycles for constant-amplitude tests and blocks for incremental-step tests.
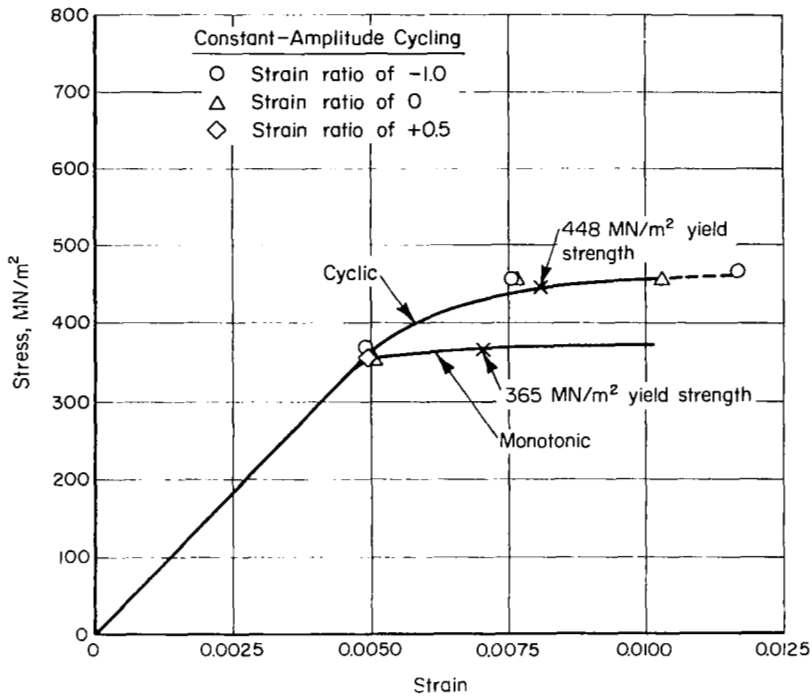
Figure A1. — Cyclic stress-strain behavior of 2024-T3 aluminum sheet.
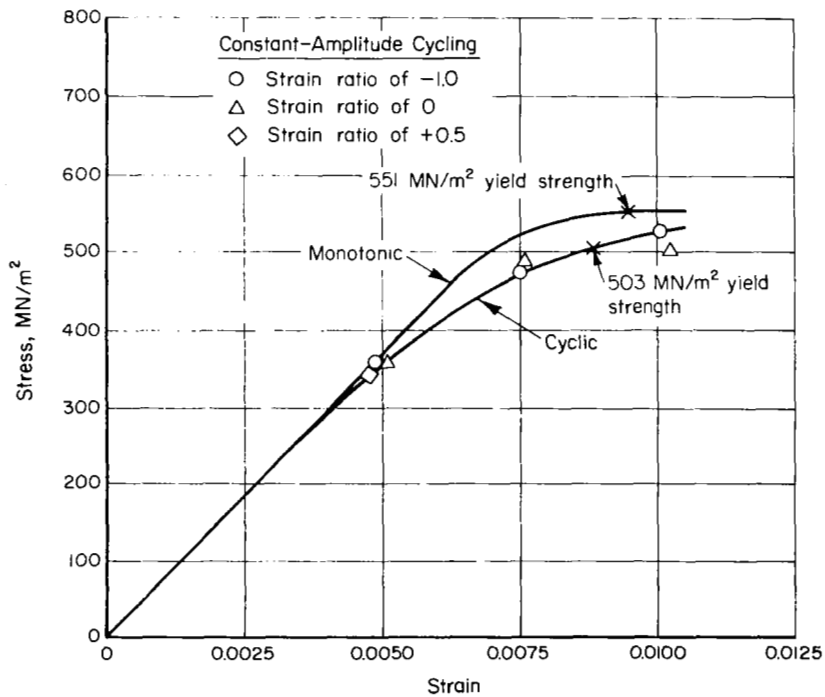
Figure A2. — Cyclic stress-strain behavior of 7075-T6 aluminum sheet.
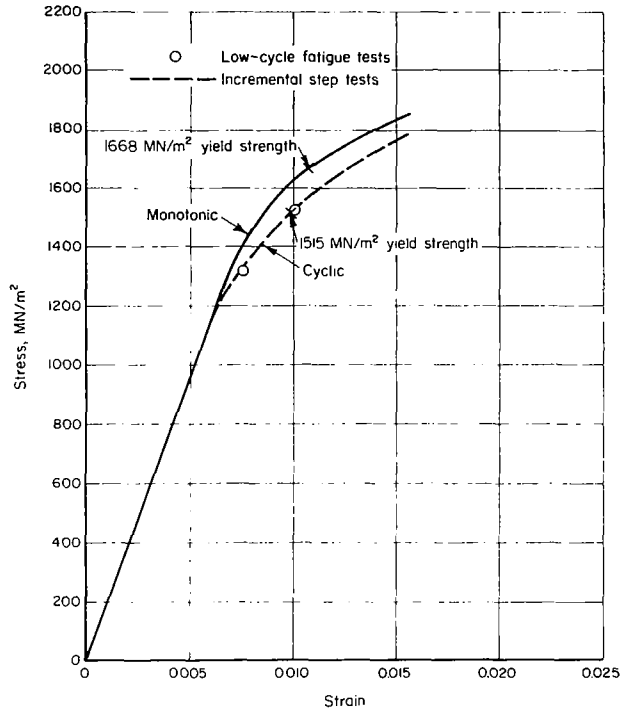
Figure A3. — Cyclic stress-strain behavior
of 300M steel forging.
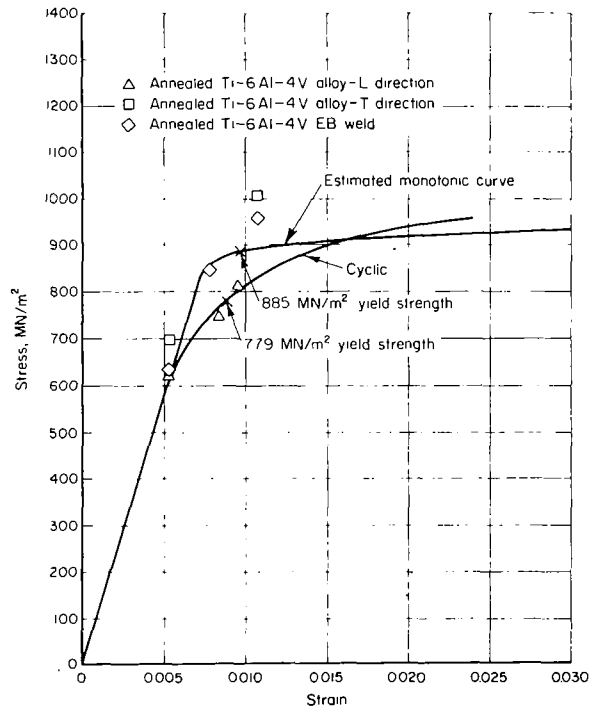
Figure A4. — Cyclic stress-strain behavior
of annealed Ti-6A1-4V plate.
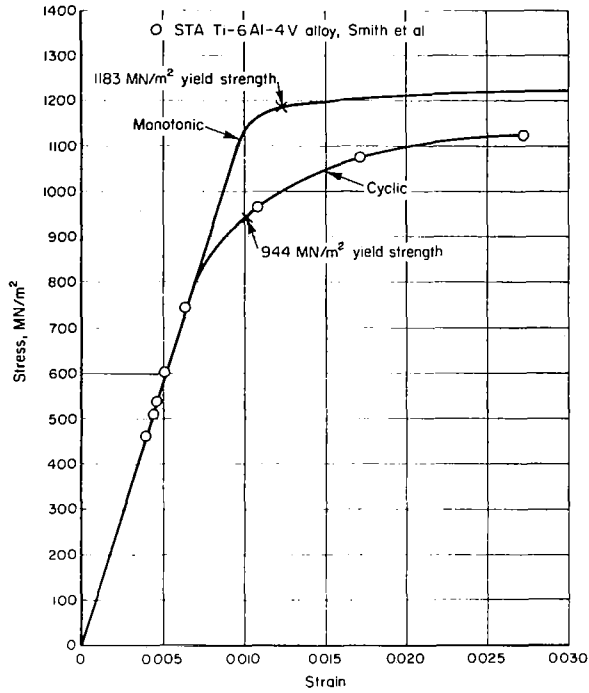
Figure A5. — Cyclic stress-strain behavior of
solution-treated and aged (STA) Ti-6Al-4V
bar, data from Smith, et al (ref. 10).
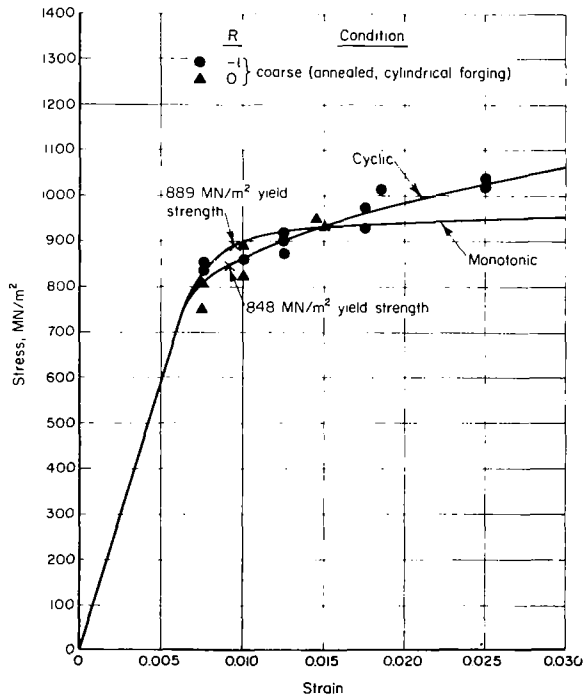
Figure A6. — Cyclic stress-strain behavior
of annealed Ti-6Al-4V forging,
data from Gamble (ref. 9).

Figure A7. — Cyclic stress-strain behavior of annealed
Ti-6Al-4V bar, data from Gamble (ref. 9).

APPENDIX B

STATISTICAL CONSIDERATIONS IN THE ANALYSIS OF
FATIGUE AND FATIGUE-CRACK-PROPAGATION DATA

The phenomenological approach to the study of fatigue and fatigue-crack propagation usually involves the formulation of a model of material behavior. In this work, the model took the form of a regression equation that was fitted to empirical data. Statistics provided the means for comparison and evaluation of the various empirical models. The following paragraphs describe the empirical models which were used and outline how they were optimized and evaluated.

In the fatigue analysis, a nonlinear model was used where necessary to describe the relationship between equivalent strain and fatigue life. The general equation form was

$$Y = B_1 X^{m_1} + B_2{}^{m_2} \tag{B1}$$

where Y represents the dependent variable, fatigue life, and X represents the independent variable, equivalent strain.

In the fatigue-crack-propagation analysis, it was possible to use a linear regression equation to describe the data as follows:

$$Y = B_0 + B_1 X \tag{B2}$$

In this case, Y represents the logarithm of crack-growth rate and X represents the transformed variable-effective stress intensity.

Optimum values of the equation coefficients (B_0 and B_1, or B_1 and B_2) were determined through least-squares regression analyses. When optimizing coefficients in equation (B1), the exponents m_1 and m_2 were fixed so that the equation could be handled through linear regression techniques. Repeated optimizations for increasingly accurate values of m_1 and m_2 gave best values for the exponents in the nonlinear expression.

The optimization procedure was based on a minimization of the standard error of estimate for the data as applied to equations (B1) or (B2). This factor was expressed as follows:

$$s_{y \cdot x} = \sqrt{\frac{\sum\limits_{i=1}^{n} (Y_i - B_0 - B_1 X_i)^2}{n - 2}} \tag{B3}$$

After the least-squares line and its parameters were established, it was of interest to know how well this line described the data. The measure of fit used in this analysis was R^2, where R is the correlation coefficient. It was calculated as follows:

$$R^2 = 1 - \frac{s_{y \cdot x}^2}{s_y^2} \tag{B4}$$

where $s_{y \cdot x}$ was determined according to equation (B3), and s_y, the sample standard deviation of Y, was calculated according to the standard formula

$$s_y = \sqrt{\frac{\sum_{i=1}^{n} (Y_i - \bar{Y})^2}{n - 1}}$$

The value of R^2, determined from equation (B4), indicated the percentage of the total variation (s_y^2) in fatigue life or crack-growth rate which was accounted for by the regression equation. A high value of R^2 (approaching 100 percent) indicates that the chosen relationship reasonably represents the underlying physical phenomenon.

Equation (B4) differs slightly from that written in the earlier presentation of this work (ref. 3). The equation presented here is the correct formulation and is the one that was actually used in all calculations.

APPENDIX C

THE INTERRELATIONSHIP BETWEEN THE EQUIVALENT STRAIN
EXPONENTS (m_1 AND m_2) AND THE UNIVERSAL-
SLOPES-TYPE EXPONENTS (b AND c)

As mentioned in the text of this report, the exponents m_1 and m_2 in the equivalent strain-fatigue life expression

$$N_f = B_1 \epsilon_{eq}^{m_1} + B_2 \epsilon_{eq}^{m_2} \tag{C1}$$

are related to the commonly used parameters, b and c, found in the following universal slopes-type equation originally recommended by Raske, et al (ref. 32).

$$\Delta\epsilon = 2^{b+1}\left(\frac{\sigma_f'}{E}\right)(N_f)^b + 2^{c+1} \epsilon_f' (N_f)^c \tag{C2}$$

The interrelationship of parameters is illustrated in figure C1 for the unnotched-specimen, 2024-T3 aluminum data examined in this study. The tri-linear logarithmic approximation of the cyclic stress-strain curve (eq. 4) is shown along with a plot of strain amplitude and equivalent strain versus fatigue life. A value of 0.40 was used for m in determination of specific values of equivalent strain. Fully reversed fatigue cycling was considered in this example, but a similar illustration could be developed for other stress ratios or mean stresses if stable values of both strain amplitude and maximum stress were available.

In the fully reversed load or strain-controlled fatigue test, a specific value of equivalent strain is definable for each point along the cyclic stress-strain curve. Since each equivalent strain value describes an expected value of fatigue life, each point on the stable cyclic σ-ϵ curve is related to a corresponding point on the ϵ_{eq}-N_f curve. The observed trend is that large strain amplitudes with corresponding stress amplitudes considerably greater than the cyclic yield strength of the material generally fall above the ϵ_{eq}-N_f curve, while smaller strain amplitudes involving little or no plastic strain fail below the ϵ_{eq}-N_f curve. Two distinct slopes are apparent for each fatigue life curve, but those slopes are dissimilar, at least in the low-cycle fatigue region. It is the intent of this brief discussion to demonstrate the interrelationships between these two fatigue life expressions in the low- and high-cycle regimes.
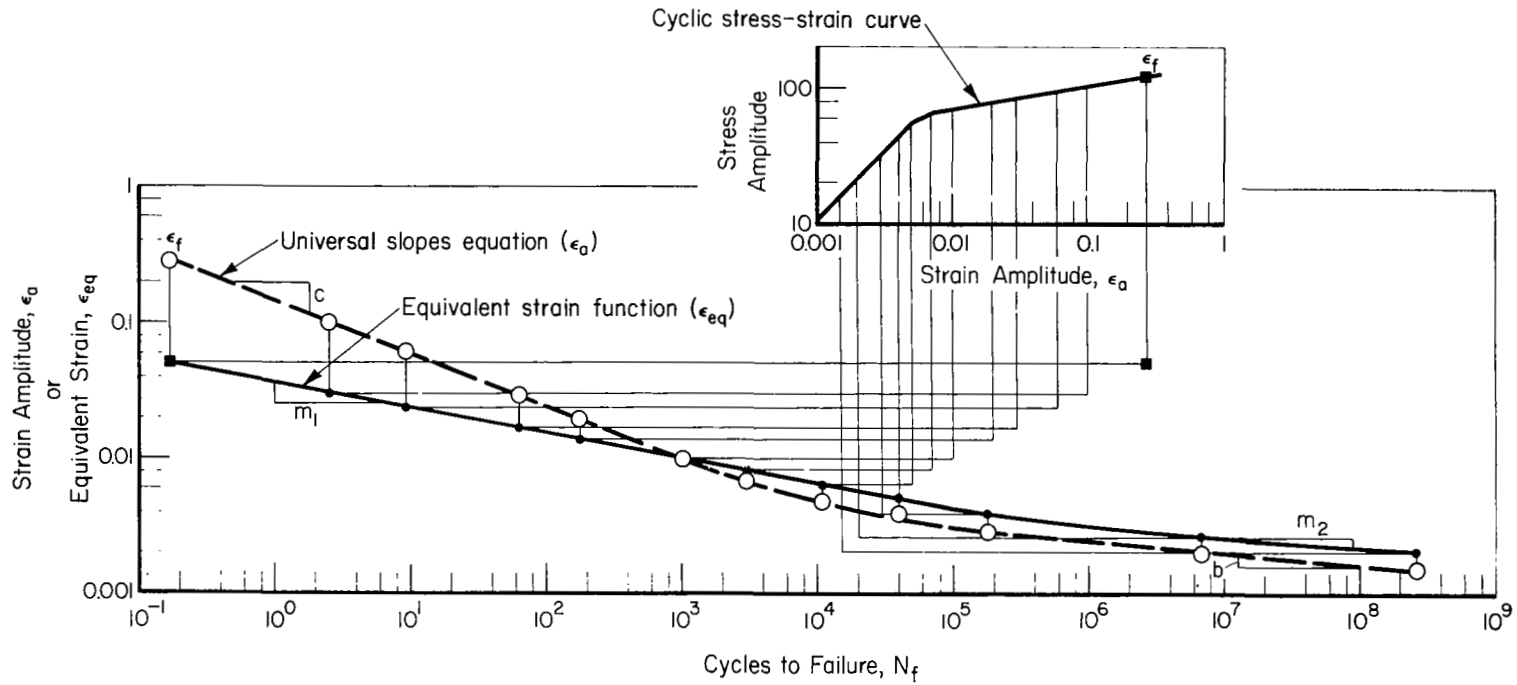
Figure C1. — Illustration of the interrelationship between the cyclic-strain curve, the equivalent strain function (ϵ_{eq}), and the universal-slopes-type equation (ϵ_a).

APPENDIX C

Low-Cycle Fatigue

For small values of N_f, where the inelastic strain range is much larger than the elastic strain range, the following approximations are reasonable.

$$N_f \simeq B_1 \epsilon_{eq}^{m_1} \qquad (C3)$$

$$\Delta\epsilon \simeq 2^{c+1} \epsilon_f'(N_f)^c \qquad (C4)$$

$$\epsilon_{eq} \simeq (\Delta\epsilon)^m \left[(\Delta\epsilon/2)^{n'} K'/E\right]^{1-m} \qquad (C5)$$

Since all three equations are simple exponentials, their logarithms may be developed and derivatives taken so that their respective logarithmic slopes may be found as follows:

$$d(\log N_f)/d(\log \epsilon_{eq}) = m_1 \qquad (C6)$$

$$d(\log \Delta\epsilon)/d(\log N_f) = c \qquad (C7)$$

$$d(\log \epsilon_{eq})/d(\log\Delta\epsilon) = m + (1-m)n' \qquad (C8)$$

A combination of these three equations also shows that the product of the slopes in the low-cycle region for the $\Delta\epsilon$-N_f and ϵ_{eq}-N_f curves should be approximately

$$cm_1 \sim 1/(m + (1-m)n') \qquad (C9)$$

Since m and n′ have been found to be about 0.40 and 0.15, respectively, for the investigated materials and c is around -0.50 for most aluminum alloys and -0.60 for several high-strength steels (ref. 33), m_1 would be expected to have a value of approximately -3.5 to -4.5. Actual optimized values of m_1 were somewhat less than this with the majority of the values for the unnotched specimen aluminum and steel data ranging from -4.5 to -7. The difference is attributable largely to the fact that very few valid data were available for $N_f < 10^3$; therefore, the slope of the ϵ_{eq}-N_f function was determined primarily by fatigue data for which the simplifying assumptions of equations (C3) and (C4) were only marginally applicable. Even if a large quantity of low-cycle-fatigue data had been available, m_1 would have been expected to have a lower value than the

estimate from equation (C9) because the exponent c applies only to plastic strain while m_1 applies to total strain.

High-Cycle Fatigue

For the large values of N_f, where the elastic strain range is much larger than the inelastic strain range, the following approximations are reasonable:

$$N_f \simeq B_2 \epsilon_{eq}^{m_2} \tag{C10}$$

$$\Delta\epsilon \simeq [2^{b+1}\sigma_f'/E] \; N_f^b \tag{C11}$$

$$\epsilon_{eq} \simeq 2^m \epsilon_a \tag{C12}$$

By taking logs and derivatives as done in the low-cycle fatigue section, it is possible to see that the logarithmic slopes of the ϵ_{eq}-N_f and $\Delta\epsilon$-N_f functions should be inversely proportional which means that the product of the slopes should be approximately equal to unity,

$$b \; m_2 \simeq 1 \tag{C13}$$

Since b is in the range of -0.09 to -0.12 for many materials (ref. 33), m_2 would be expected to fall in the range of -8 to -11. Actual optimized values were again somewhat lower than this with slopes for unnotched specimen data ranging from -13 to -16. The low values of m_2 are partially due to the corresponding low values of m_1. The exponent m_1 in the first term of equation (C1) causes the optimum values of m_2 to increase if it is raised and decrease if it is lowered. Optimum values for m_1 and m_2 cannot be independently selected. The primary exponent m_1 should first be optimized and then the secondary exponent m_2 should be set at an optimum or reasonable value. In some cases where only a small quantity of high-cycle fatigue data are available, the second term (and m_2) in equation (C1) may be eliminated entirely with no reduction in quality of the overall data representation.

REFERENCES

1. Anon.: Military Standardization Handbook, Metallic Materials and Elements for Aerospace Vehicle Structures. MIL-HDBK-5B, 1971.

2. Anon.: Tentative Recommended Practice for Constant-Amplitude Axial Fatigue Tests of Metallic Materials. ASTM Designation E-466-72T. Annual Book of ASTM Standards, Part 31, 1973.

3. Jaske, C. E.; Feddersen, C. E.; Davies, K. B.; and Rice, R. C.: Analysis of Fatigue, Fatigue-Crack Propagation and Fracture Data. NASA CR-132332, 1973.

4. Walker, K.: The Effect of Stress Ratio During Crack Propagation and Fatigue for 2024-T3 and 7075-T6 Aluminum. Effects of Environment and Complex Load History on Fatigue Life. Spec. Tech. Publ. 462, ASTM, 1970, pp. 1-14.

5. Smith, K. N.; Watson, P.; and Topper, T. H.: A Stress-Strain Function for the Fatigue of Metals. J. Matl., vol. 5, no. 4, December 1970, pp. 767-778.

6. Topper, T. H.; and Sandor, B. I.: Effects of Mean Stress and Prestrain on Fatigue-Damage Summation. Effects of Environment and Complex Load History on Fatigue Life. Spec. Tech. Publ. 462, ASTM, 1970, pp. 93-104.

7. Endo, T.; and Morrow, JoDean: Cyclic Stress-Strain and Fatigue Behavior of Representative Aircraft Metals. J. Matl., vol. 4, no. 1, March 1969, pp. 159-175.

8. Landgraf, R. W.; Morrow, JoDean; and Endo, T.: Determination of the Cyclic Stress-Strain Curve. J. Matl., vol. 4, no. 1, March 1969, pp. 176-188.

9. Gamble, R. M.: The Effect of Microstructure on the Tensile Properties, Low-Cycle Fatigue Life, and Endurance Limit of Annealed Titanium Alloy 6Al-4V. M.S. Thesis, Univ. of Fla., 1972.

10. Smith, R. W.; Hirschberg, M. H.; and Manson, S. S.: Fatigue Behavior of Materials Under Strain Cycling in Low and Intermediate Life Range. NASA TN D-1574, 1963.

11. Wetzel, R. M.: Smooth Specimen Simulation of Fatigue Behavior in Notches. J. Matl., vol. 3, no. 3, September 1968, pp. 646-657.

12. Topper, T. H.; Wetzel, R. M.; and Morrow, JoDean: Neuber's Rule Applied to Fatigue of Notched Specimens. J. Matl., vol. 4, no. 1, March 1969, pp. 200-209.

13. Morrow, JoDean; Wetzel, R. M.; and Topper, T. H.: Laboratory Simulation of Structural Fatigue Behavior. Effects of Environment and Complex Load History on Fatigue Life. Spec. Tech. Publ. 462, ASTM, 1970, pp. 74-91.

14. Morrow, JoDean; Martin, J. F.; and Dowling, N. W.: Local Stress-Strain Approach to Cumulative Fatigue Damage Analysis. Report No. 379, Theoretical and Applied Mechanics, Univ. of Ill., January 1974.

15. Stadnick, S. J.; and Morrow, JoDean: Techniques for Smooth Specimen Simulation of the Fatigue Behavior of Notched Members. Testing for Prediction of Material Performance in Structures and Components. Spec. Tech. Publ. 515, ASTM, 1972, pp. 229-252.

16. Peterson, R. E.: Stress Concentration Design Factors. John Wiley and Sons, Inc., New York, 1953.

17. Neuber, H.: Theory of Stress Concentration Shear Strained Prismatical Bodies With Arbitrary Nonlinear Stress-Strain Law. J. Appl. Mech., December 1961, pp. 544-550.

18. Peterson, R. E.: Notch-Sensitivity. Metal Fatigue. Sines, G.; and Waisman, J. L., eds.: McGraw-Hill Book Co., 1959, pp. 293-306.

19. Raske, D. T.: Section and Notch Size Effects in Fatigue. T. & A. M. Report No. 360, Univ. of Ill., 1972.

20. Rice, R. C.; and Jaske, C. E.: Consolidated Presentation of Fatigue Data for Design Applications. Society of Automotive Engineers Preprint No. 740277, March 1974.

21. Manson, S. S.: A Simple Procedure for Estimating High-Temperature, Low-Cycle Fatigue. Experimental Mechanics, vol. 8, no. 8, August 1968, pp. 349-355.

22. Jacoby, G. H.; and Nowack, H.: Comparisons of Scatter Under Program and Random Loading and Influencing Factors. Probabilistic Aspects of Fatigue. Spec. Tech. Publ. 511, ASTM, 1972, pp. 61-74.

23. Bastenaire, F. A.: New Method for the Statistical Evaluation of Constant Stress Amplitude Fatigue-Test Results. Spec. Tech. Publ. 511, ASTM, 1972, pp. 3-28.

24. Draper, N. R.; and Smith, H.: Applied Regression Analysis. Wiley Publications in Statistics, 1966.

25. Owen, D. B.: Factors for One-Sided Tolerance Limits and for Variables and Sampling Plans. Sandia Corporation Monograph SCR-607, March 1963.

26. Hildebrand, F. B.: Introduction to Numerical Analysis. McGraw-Hill Publishing Co., New York, 1956, pp. 43-45.

27. Erdogan, F.: Crack Propagation Theories. NASA CR-901, October 1967.

28. Hoskin, B. C.: Simple Theoretical Studies of Fatigue-Crack Propagation Using a Fracture Mechanics Approach. NTIS N72-28897, December 1971.

29. Coffin, L. F.: Fatigue, Annual Review Material Science, vol. 2, 1972, pp. 313-348.

30. Collipriest, J. E.: An Experimentalist's View of the Surface Flaw Problem. The Surface Crack: Physical Problems and Computational Solutions. ASME, 1972, pp. 43-62.

31. Jaske, C. E.; Mindlin, H.; and Perrin, J. S.: Cyclic Stress-Strain Behavior of the Alloys at High Temperature. Cyclic Stress-Strain Behavior Analysis, Experimentation, and Failure Prediction. Spec. Tech. Publ. 519, ASTM, 1973, pp. 13-27.

32. Raske, D. T.; and Morrow, JoDean: Mechanics of Materials in Low-Cycle Fatigue Testing. Manual on Low-Cycle Fatigue Testing. Spec. Tech. Publ. 465, ASTM, 1969, pp. 1-25.

33. Tucker, L. E.; Landgraf, R. W.; and Brose, W. R.: Proposed Technical Report on the Fatigue Properties for the SAE Handbook, SAE Tech. Report 740279, March 1974.